8-2015

Design of a Neuromemristive Echo State Network Architecture

Qutaiba Mohammed Saleh

Recommended Citation

Saleh, Qutaiba Mohammed, "Design of a Neuromemristive Echo State Network Architecture" (2015). Thesis. Rochester Institute of Technology. Accessed from

Design of a Neuromemristive Echo State Network Architecture

by

Qutaiba Mohammed Saleh

A Thesis Submitted in Partial Fulfillment of the Requirements for the Degree of Master of Science
in Computer Engineering

Supervised by

Associate Professor Dr. Dhireesha Kudithipudi
Department of Computer Engineering
Kate Gleason College of Engineering
Rochester Institute of Technology
Rochester, New York
August 2015

Approved by:

Dr. Dhireesha Kudithipudi, Associate Professor
Thesis Advisor, Department of Computer Engineering

Dr. Andres Kwasinski, Associate Professor
Committee Member, Department of Computer Engineering

Dr. Ray Ptucha, Assistant Professor
Committee Member, Department of Computer Engineering

Thesis Release Permission Form

Rochester Institute of Technology
Kate Gleason College of Engineering

Title:

Design of a Neuromemristive Echo State Network Architecture

I, Qutaiba Mohammed Saleh, hereby grant permission to the Wallace Memorial Library to reproduce my thesis in whole or part.

Qutaiba Mohammed Saleh

Date

Dedication

To my beloved family, for all of your support along the way.

Acknowledgments

I am grateful for my thesis advisor Dr. Dhireesha Kudithipudi. I could not have achieved this without her invaluable motivation, patience, and dedication to this work. I also thank Dr. Andres Kwasinski and Dr. Ray Ptucha for serving on my thesis committee and their insightful comments and encouragement. Furthermore, I thank the rest of the department faculty and staff for their support through my study.

I thank my labmates Cory Merkel, Colin Donahue, James Manatzaganian, Levs Dolgovs, and James Thesing for their guidance and the stimulating discussions. Finally, I would like to thank the Iraqi Ministry of Higher Education and Scientific Research for the full scholarship to complete my Master study.

Abstract

Design of a Neuromemristive Echo State Network Architecture

Qutaiba Mohammed Saleh

Supervising Professor: Dr. Dhireesha Kudithipudi

Echo state neural networks (ESNs) provide an efficient classification technique for spatiotemporal signals. The feedback connections in the ESN enable feature extraction in both spatial and temporal components in time series data. This property has been used in several application domains such as image and video analysis, anomaly detection, and speech recognition. The software implementations of the ESN demonstrated efficiency in processing such applications, and have low design cost and flexibility. However, hardware implementation is necessary for power constrained resources applications such as therapeutic and mobile devices. Moreover, software realization consumes an order or more power compared to the hardware realization. In this work, a hardware ESN architecture with neuromemristive system is proposed. A neuromemristive system is a brain inspired computing system that uses memristive devises for synaptic plasticity. The memristive devices in neuromemristive systems have several interesting properties such as small footprint, simple device structure, and most importantly zero static power dissipation. The proposed architecture is reconfigurable for different ESN topologies. 2-D mesh architecture and toroidal networks are exploited in the reservoir layer. The relation between performance of the proposed reservoir architecture and reservoir metrics are analyzed. The proposed architecture is tested on a suite of medical and human computer interaction applications. The benchmark suite includes epileptic seizure detection, speech emotion recognition, and electromyography (EMG) based finger motion recognition. The proposed ESN architecture demonstrated an accuracy of 90%, 96%, and 84% for epileptic seizure detection, speech emotion recognition and EMG prosthetic fingers control respectively.

Contents

List of Tables

List of Figures

Chapter 1

Introduction

1.1 Motivation

Spatiotempporal signals have been widely used in various of applications such as speech recognition, video and music editing, and bio-signal processing. These signals are processed based on their behavior in time series windows. For example, the goal of speech recognition is translating an audio signal into text. Observing the signal at a specific time does not provide enough information for translation. Taking multiple measurements of the signal in a time series window provides the required information to describe the speech. Reservoir computing has been heavily used in processing spatiotemporal signals. The recurrent connections of the reservoir layer enable extracting desired features within a time frame [36]. These random connections make the state of the reservoir layer oscillate at the edge of chaos [7], which is region of dynamic systems that operates at the boundary between chaotic and non-chaotic behavior [34]. This property has been utilized in several reservoir computing models.

Echo State Network (ESN) is a type of reservoir computing neural network in which the reservoir state depends on current the input and all the previous inputs to the reservoir layer [23]. It has a simple training algorithm compared to other types of recurrent neural networks [34]. The software implementations of the ESNs are effective in diverse

---

The words ESN and Reservoir are used interchangeably in this document.

applications offering low cost and flexible designs. These software ESN models are implemented on conventional computing systems (such as Von Neumann systems). Such systems demand large area to fit the design and consume considerable power to run different components on the chip. Primarily, Von Neumann systems are not design for processing limited resources applications such as body sensors, therapeutic, and mobile devices. Such applications require processing models that have low power consumption, small area and high processing speed. For example in smart phones, power consumption is critical [11]. Supporting such devices with large batteries may solve the power consumption problem in some applications. However, this solution can not be considered for therapeutic and body sensors where the device is physically attached to the patients. These devices also require real-time processing speed to detect any event in the tested bio-signals and take the appropriate action.

A custom hardware implementation of ESN is preferred to meet these requirements. Several approaches to implement hardware neural networks have been presented. Like the software implementation, the digital hardware approach has flexibility and ease of implementation. It also partially satisfies some of the critical requirements addressed before. The neuromorphic computing approach can more effectively meet these requirements. It is a non-conventional system built of mixed signal hardware circuits inspired by the human brain [38]. Neuromophic designs have several appealing properties over the traditional CMOS implementations in terms of power consummation, area, speed, and cost [19]. It also offers highly parallel architectures. Neuromemristive systems are a class of meromorphic computing [2]. It uses memristive devices for synapses implementations. The memristor is a passive electrical component that has a variable resistance depending of the internal state [13]. The resistance values of the devices are changed based on the duration and amount of current flow through it. This memory property is used to save the weight value or strength of the synaptic connection in neuromorphic designs.

Building a neuromorphic architecture model of ESN using memrisive devices will satisfy the requirements of low power consumption, small area and high processing speed. Such an architecture fills a knowledge gap in hardware reservoir designs, which operate in real-time with limited power resource applications. Medical devices are in the top of list of applications that can benefit from these systems. These devices are used by wide range of medical professionals to diagnose diverse set of diseases and infections such as epileptic seizure, neuromuscular diseases, kinesiology, motor control disorders, and emotional disorders.

1.2 List of Objectives

- Develop a software ESN model for baseline analysis.
- Design a hardware neuromemristive ESN model, with varying reservoir topologies (random, ring, and hybrid).
    - Design an ESN model using memristive-based synapse circuits as building blocks.
    - Design a novel hybrid reservoir topology.
    - Implement the neuromemristive reservoir on a set of different reservoir topologies.
    - Optimize this model for parameters such as reservoir layer size, degree of connectivity, and alpha.
    - Analyze the correlation between reservoir metrics and performance.
- Hardware architecture for the memristive reservoir.
    - A homogeneous, scalable, and reconfigurable architecture that is used as a platform to implement the reservoir.
    - Two architectures are used to design this platform: Mesh networks and doubly twisted toroidal networks.
- Use the proposed neuromemristive architecture to build complete processing platforms for three applications:
    - Epileptic seizure detection using Electroencephalogram signals (EEG).

  - Speech emotion recognition. Use speech to detect two emotions: neutral and anger.
  - Prosthetic finger control using surface electromyogram signals (EMG).

1.3 Summary

The reset of this document is outlined as follows: Chapter 2 gives an introduction of ESN and its training algorithm and demonstrates an example. It also presents the related work in the literature. Chapter 3 discusses the memristive synapse and neuronal circuits used in this work. Chapter 4 presents the proposed neuromemristive architecture and the modified novel hybrid reservoir topology. Chapter 5 describes the benchmarks that are used to test the proposed architecture and the feature extractors. The simulation results obtained from applying these benchmarks and the metrics analysis are presented in Chapter 6. Chapter 7 discusses conclusions and future work.

Chapter 2

Background and Related Work

2.1 Introduction to Echo State Networks

Echo State Network (ESN) is a class of reservoir computing model presented by Jaeger *et al.* in 2001 [21]. ESNs are considered as partially-trained artificial neural networks (ANNs) with a recurrent network topology. They are used for spatiotemporal signal processing problems. The ESN model is inspired by the emerging dynamics of how the brain handles temporal stimuli. It consists of an input layer, a reservoir layer and an output layer (see Figure 2.1). The reservoir layer, is the heart of the network, with rich recurrent connections. These connections are randomly generated and each connection has a random weight associated with it. Once generated, these random weights are never changed during training or testing phases of the network. The output layer of the ESN linearly combines the desired output signal from the rich variety of excited reservoir layer signals. The central idea is that only the network to the output layer connection weights have to be trained, using simple linear regression algorithms. Another reservoir model, known as liquid state machine, provides a biologically plausible model for generating computations in cortical microcircuits. In contrast, ESN provides a high performance mathematical framework for solving a number of engineering tasks. Specifically, they can be applied to recurrent artificial neural networks without internal noise. ESNs have simplified training algorithms compared to other recurrent ANNs and are more efficient than kernel-based methods (e.g.: Support Vector Machines) due to their ability to incorporate temporal stimuli. Because of its recurrent connections, the output of the reservoir depends on the current input state and all previous input states within the system memory. The recurrent network topology of the reservoir enables feature extraction of spatiotemporal signals. This property has been used in several application domains such as image and video analysis, anomaly detection, and speech recognition.

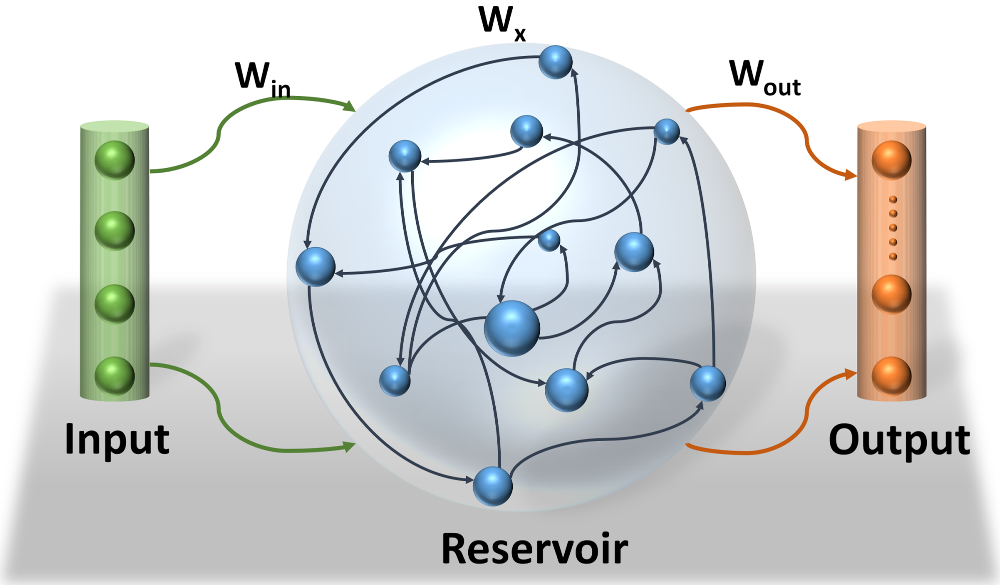

Figure 2.1: An Echo State Network consists of three layers: input layer, reservoir layer and output layer

2.1.1 Training Algorithm

Three main sets of weights are associated with the ESNs (Figure 2.2). The weights at the input and reservoir layers are randomly generated. These layers are used to extract temporal features of the input signal. They can be thought of as an internal pre-process step that prepares the signal for the actual processing layer where the classification is learned at the readout layer. Figure 2.2 also shows the propagation of the signals through the ESNs. The input signal to the ESN $u[n]$ is pre-processed at the input and reservoir layers to extract the temporal featured signal $x[n]$ which is fed to the readout layer to complete the classification process. Considering that the input and reservoir layers are not actual parts of this process, their weights are not trained which makes training the ESNs much easier than other types of recurrent neural networks.

The goal of the training algorithm is to calculate the weights at the output layer based

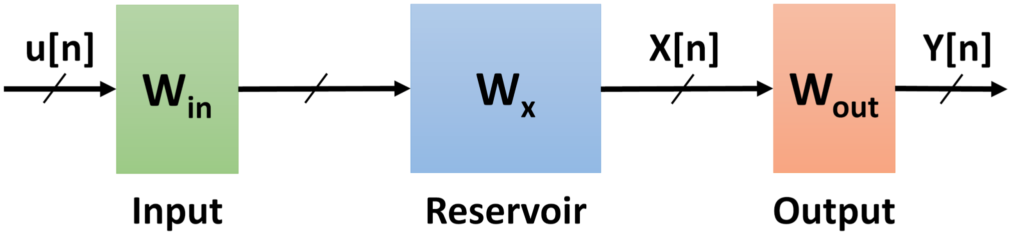

Figure 2.2: Echo State Networks abstract structure. How signals propagate through the ESN and the effects of different weight sets in the network.

on the dynamic response (states) of the reservoir layer [22]. The states of the reservoir layer are calculated based on the input vectors and the weights of the input and reservoir layer as shown in (2.1).

$$\mathbf{x}[n+1] = f^{\text{res}}\left(\mathbf{W}_{\text{in}}\mathbf{u}[n+1] + \mathbf{W}_{\text{x}}\mathbf{x}[n]\right) \tag{2.1}$$

where $\mathbf{u}[n]$ is the ESN input, $\mathbf{W}_{\text{in}}$ is the weight matrix between the input layer and reservoir layer, $\mathbf{W}_{\text{x}}$ is the weight matrix between the neurons within the reservoir layer, and f^{res} is the reservoir layer's activation function.

The states of the reservoir layer for all input vectors are used as an input to a supervised training to calculate the output weights $\mathbf{W}_{\text{out}}$. There are several linear regression methods to calculate the weights at the output layer. This work uses normal equation to implement the supervised training of the ESN (2.2).

$$\mathbf{W}_{\text{out}} = (\mathbf{Y}\mathbf{X}')(\mathbf{X}\mathbf{X}')^{-1} \tag{2.2}$$

where $\mathbf{X}$ is a matrix concatenating all states of the reservoir layer and $\mathbf{Y}$ is a matrix of all training outputs.

The process for training the ESN can be explained through the following steps:

1. At initialization, randomly generate the weights for the input and reservoir layers ($\mathbf{W}_{\text{in}}$ and $\mathbf{W}_{\text{x}}$)

2. Drive the next input vector $\mathbf{u}[n+1]$ to the input layer

3. Calculate the response of the reservoir layer by 2.1
4. Save the response in a matrix ($\mathbf{X}$)
5. Repeat step 2-4 for all input vectors
6. Calculate output weights based on normal equation 2.2

Once the weights of the output layer are calculated, the network is ready and the state of the reservoir layer is used to calculate the output of the network as shown in (2.3).

$$\mathbf{y}[n+1] = f^{\text{out}}\left(\mathbf{W}_{\text{out}}\mathbf{x}[n+1]\right) \tag{2.3}$$

where $\mathbf{y}[n+1]$ is the output of the network, $\mathbf{W}_{\text{out}}$ is the weight matrix at the readout layer and f^{out} is the readout layer's activation function.

2.1.2 Training Example

This example elucidates how an ESN can be trained to classify temporal signals. A single-channel sinusoid input signal $u(n) = sin(2\pi F n)$ is used. This signal periodically oscillates at two different frequencies F_1 and F_2. The ESN in this example is used to classify the input sinusoid signal based on its frequency. For such problem, a single output unit is enough to represent the two classes F_1 and F_2. Since the problem is simple and has uncomplicated features based on which the decision is made, a small reservoir layer is used. The network used consists of single input unit, 20 reservoir units and a single output unit. The values of the signal frequencies F_1 and F_2 are 4 and 2 Hz respectively. The signal is sampled at a rate of 100 Hz. The target output of the network is -1 for F_1 and 1 for F_2. The algorithm described in the previous section is used to train the network for this classification problem.

Figure 2.3 shows the propagation of the signal through the ESN starting from the input tested signal Figure 2.3(a). It also shows the responses of the reservoir layer to this input signal figure 2.3(b). As can be seen, the reservoir layer's response varies based on the input signal in both frequency and amplitude. The variations of the signals at the output of the reservoir layer represent extracted features based on which classification decision is made at the output layer. Figure 2.3(c) is the output signal at the output layer. This signal is compared to some threshold value to generate the final output as seen in figure 2.3(d).

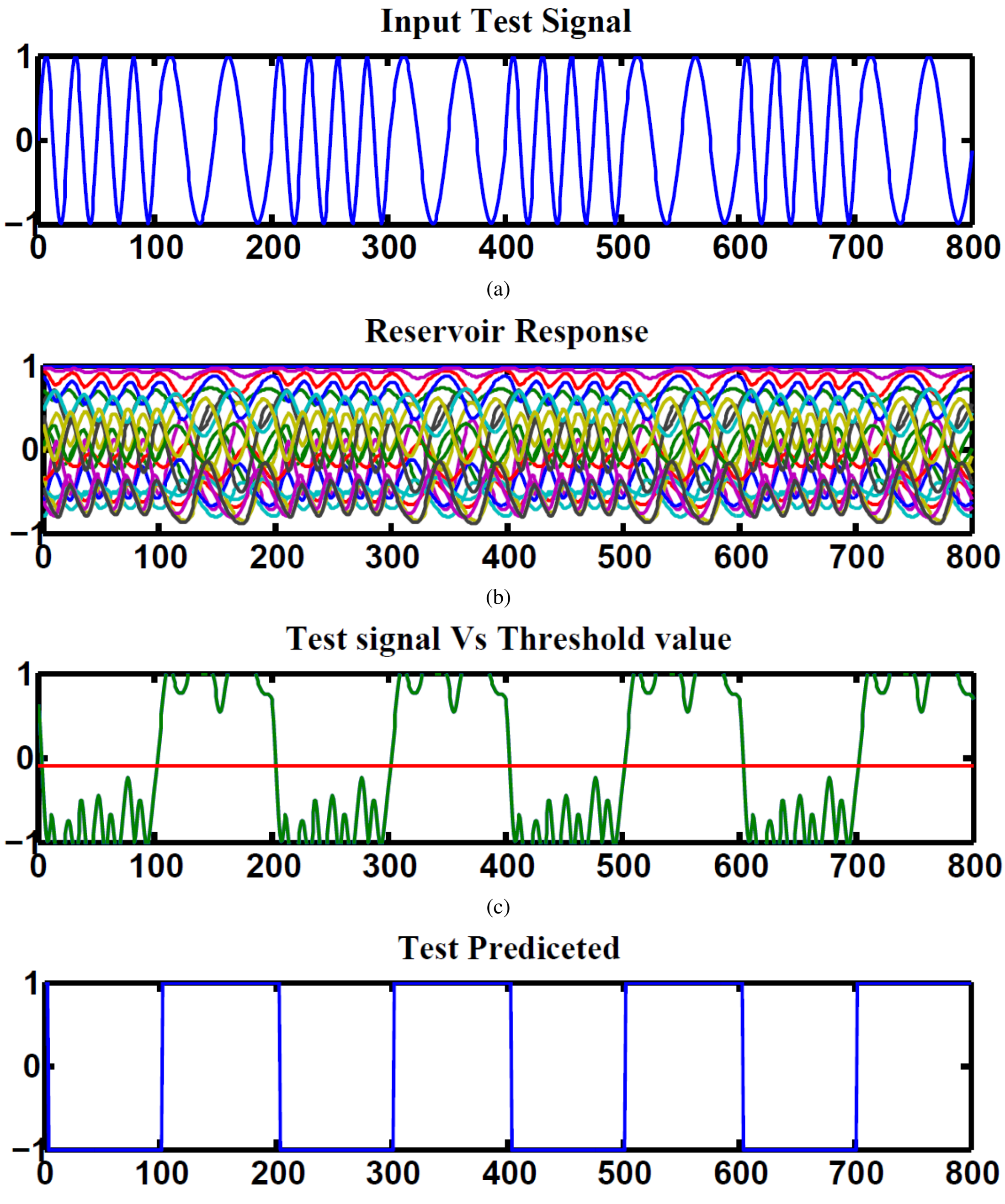

(a)

(b)

(c)

(d)

Figure 2.3: Signals propagation through the tested ESN over time. The plots shows (a) input sinusoid test signal, (b) reservoir layer responses to this signal, (c) output signal of the ESN and (d) final classification signal.

Different threshold values are used to increase the classification accuracy. Figure 2.4 shows the training and testing accuracy vs. different threshold values. The maximum accuracy achieved is 98%. This example is a simple demonstration of how ESNs are powerful at processing temporal signals.

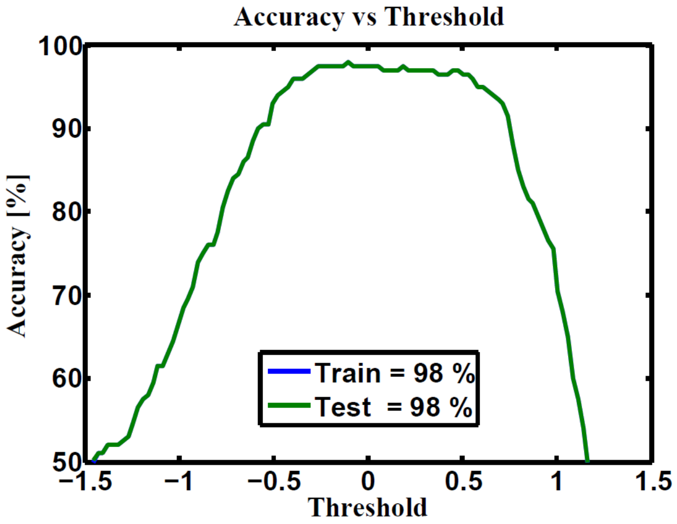

Figure 2.4: Training and testing classification accuracies of the sinusoid signal verses different threshold values. The maximum accuracy achieved for both training and testing is 98%.

2.2 Related work

2.2.1 Applications

The software implementations of the ESN have been effective at diverse applications such as emotion recognition [52], forecasting of water inflow for a hydropower plant [49], natural language analysis [57], motion identification [20], speech recognition [54], and many more applications (see [35] for a review). The previous work on the applications used in this project is explored in the next sections.

2.2.2 Epileptic Seisure Detection

Epileptic Seizure detection is one of the biomedical applications that was implemented using ESNs. Epileptic seizures are chronic disorders of the central nervous system, where one in 26 people will develop this disorder at sometime in their life [1]. It can be often detected through analysis of electroencephalogram (EEG) signals. A software ESN model for epileptic seizure detection is presented in [8]. The reservoir layer in the design consists of 200 randomly connected neuronal nodes with 90% connectivity. The EEG dataset used for testing purposes was taken from rats which have behavioral similarity with human EEG signals. The input signal is pre-processed before it is fed to the actual ESN. Similarly, the output signal of the ESN passes through a post process stage before the final decision is made. This model showed fast and accurate results compared to other methods that use non ESN techniques. The results in this work showed that ESNs are more effective in processing EEG signals for epileptic seizure detection. However, the software model presented in this work has high number of neuronal nodes with high degree of connectivity. These two properties are not desired for hardware implementations [48]. On the other hand the pre-process stage and its relation with the reset of the model was not fully explained in the paper. A full system level implementation with design details are not presented. Moreover, the EEG signals used for validation were confidential data and can not be compound or used by other researchers.

2.2.3 Emotion Recognition

In emotion recognition, the emotional status of a human like anger, fear, happiness etc are detected. Human-computer interaction is an application of emotion recognition [15]. Using this property, computers can have better interaction with human. Using speech for emotion recognition requires lower computational resources compared to other inputs as facial expressions.

The software ESN model introduced in [52] uses features like energy, pitch and speech spectral base features to recognize emotions. The Mel Frequency Cepstral Coefficients (MFCC) are used for emotional feature extraction. The extracted features are used to train the ESN network. A reservoir layer of 500 neuronal nodes with 50% degree of connectivity is used in this ESN. The model was able to detect two different emotional statuses (natural and anger) with an accuracy of 99%. This accuracy was achieved in real-time speed. The results proved that ESNs are a viable option for emotion recognition. These results can be tested considering that the dataset used is publicly available. The pre-process stage (feature extractor) is also well explained while exhibiting all similar techniques in the literature. The paper showed that the recognition speed was fast enough to be used in real-time applications without explaining the characteristics of the computing system used in the experiment. The work presented in this paper can be improved to detect more emotional statuses so that it can be considered as a stand-alone recognition system. The ESN model presented in this paper has acceptable degree of connectivity for a hardware implementation. The pre-process stage can be also considered for such implementation.

2.2.4 Electromyography

Electromyography (EMG) is a biosignal collected by measuring muscles potential activities. EMG signals are recorded using electrodes sensors. With the advances of signal processing techniques, EMG signals have been used for several medical applications such as neuromuscular disorder diagnosis and prosthetic devices control. Processing of EMG signals can be summarized into three steps: signals decomposition, feature extraction, and signal classification [46].

Several traditional statistical techniques have been used for EMG signal processing such as Linear Discrimination Analysis (LDA), Quadratic Discriminant Analysis (QDA), Gaussian Mixture Models (GMM), Hidden Markov Models (HMM), and k-Nearest neighbor classifier (refer to [61] for more examples). Khushaba *et al.* [27] used support vector machine (SVM), k-Nearest neighbor, and extreme learning machine (ELM) to classify fifteen finger movements of the upper limbs. Artificial neural network classifier models have also been used for EMG signals. These models include MLP, back-propagation network, conic section function neural network, and fuzzy clustering neural network [24]. Subasy *et al.* used neural networks to detect two types of neuromuscular disorders: myopathy and neurogenic disease [56]. The classification accuracy of EMG signals are 90.7% and 88% for feedforward error back-propagation (FEB) and wavelet neural networks (WNN) respectively. This work classifies EMG signals based on finger motions for prosthetic finger control. To the best of my knowledge, not only is this the first work presenting a neuromemristive architecture to classify EMG signals but it also the first work processing this class of signals using reservoir computing.

2.2.5 Hardware Reservoir Models

Software implementations proved that ESNs are efficient in different application domains. However, the software models are not efficient for embedded and low-end processing environments, where power dissipation is critical to the operation of the devices. A few research groups presented hardware ESN models based on memristive devices. Next are two examples that used memristive devices to build reservoir models.

Kulkarni *et al.* in [29] presented a memristor-based reservoir model. The memristive devices in this model are used as building blocks to construct the reservoir layer. They are considered as bi-directional connections that are randomly connected based on graph theory approach to generate different reservoir topologies. In this architecture, each memristive device represents an edge that connects two nodes or vertices in the graph Figure 2.5(b). Except for a self loop connection, each node can be connected to any other node in the graph. The existence of a connection between two nodes means a new memristive device is added to the circuit. The responses of the reservoir are taken from these nodes. Figure 2.5(b) shows a circuit representation of reservoir generated base on graph theory. The reservoir layer was modeled in Ngspice while the output layer was trained using genetic algorithm. The work presents a generic reservoir model. While it provides a good explanation of the theoretical algorithm to establish the reservoir topology, it gives no specification of the type of the reservoir (example Liquid State Machine (LSM) or ESN) where each reservoir type has its own characteristics in terms of weight generation and activation functions. It neither gives details of the circuits at the output layer nor how the weight values have been trained. At the same time no power or performance measurements were presented in this work. Except for some simple classification problems, the model was not used for a specific application.

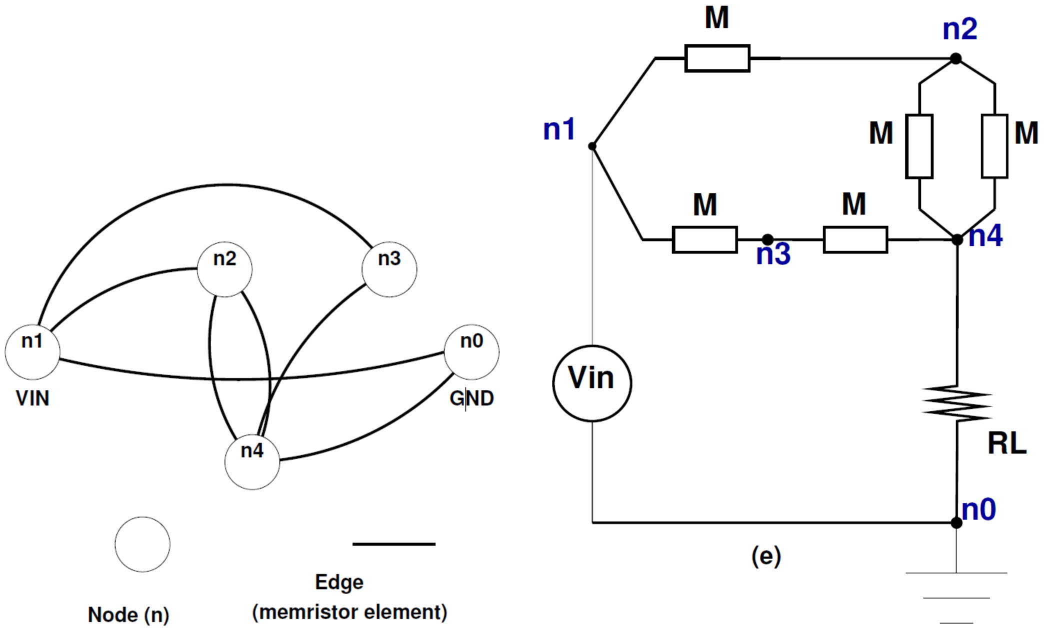

(a) (b)

Figure 2.5: (a) Graph representation of a random reservoir. Edges represent memristors and nodes represent neurons in the reservoir. (b) Circuit representation [29].

Burger *et al.* presented a structured memristive reservoir architecture in [5]. The memristive devices are connected as a mesh network. The effect of process variations of the devices is used to set the random weight values of the reservoir synapses. The device-to-device variation gives each memristor its unique maximum and minimum resistances and threshold voltages. The topology consists of a matrix of nodes that are connected by memristors as a mesh network Figure 2.6. One of the nodes is selected to be an input node that is used to feed the input signal into the reservoir. The rest of the nodes are used as outlets where the response of the reservoir is measured. As in any reservoir computing model, the response of the reservoir layer is used to train the output layer. The output layer is implemented in software as step function perceptrons. Genetic algorithm is used to train the output layer to overcome the problem of local minima in a given search space.

Five different sizes of reservoirs were simulated to study the relationship between reservoir size, number of memristive devices, and the performance. The performance of this work is compared with the performance of the model presented in [29] which uses a random reservoir topology. In this experiment, both mesh and random architectures use the process variation to generate the weights of the reservoir layer. These architectures were trained to classify a frequency modulated signal that has two frequencies. The experiment revealed that the reservoir is tolerant to the process variation. It also showed that increasing the size of the reservoir improves the variation tolerance and decreases the error rate for both mesh and random architectures. The overall performance of the two tested architectures have the same response toward changing the degree of variation and size of the reservoir but in general the regular mesh architecture showed better performance compared to the random architecture.

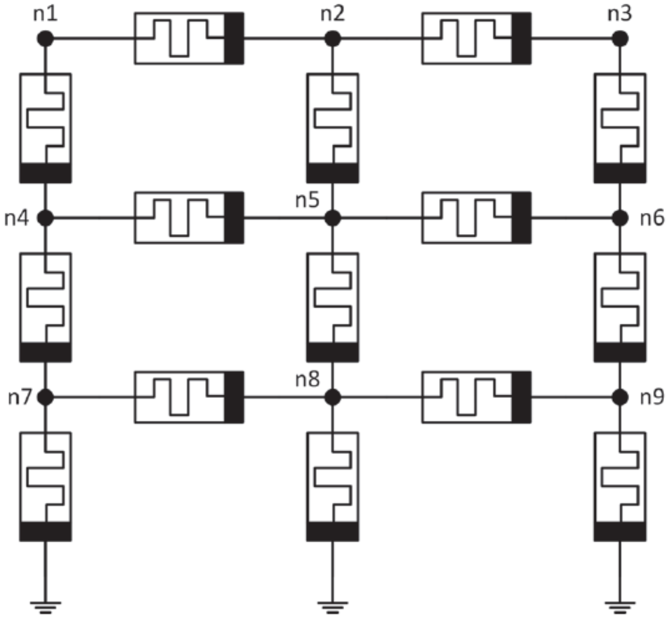

Figure 2.6: Reservoir architecture as presented in [5]. It is a regular mesh network connecting a number of nodes using memristors as links.

This work presents a homogeneous architecture that was analyzed for different parameters. It uses, however, a simple classification problem. More complicated applications that has high impacts on industry and human life could have been used to validate the architecture. Such applications empower the architecture and present it as a possible solution for daily faced problems. No metrics are used to analyze the effectiveness of the reservoir in any of these works.

2.3 Summary

ESN is a class of reservoir computing, which processes information based on its behavior history. This property presents ESN as a powerful candidate for processing spatiotemporal signals. Epileptic seizure detection and speech emotion recognition are two examples applied on software ESN models. Hardware ESN, however, is not a well explored area. There is a few memristive based ESN architectures presented in the literature. These architectures were not tested on vital well defined applications. This work presents a neuromemristive ESN architecture and uses it for epileptic seizure detection, speech recognition, and EMG signals processing. To the best of my knowledge, this is the first ESN model that processes EMG and combines it with EEG and speech emotion recognition.

Chapter 3

Circuit Models

From a circuit point of view, an ESN consists of a number of neurons connected by a set of synapses in a specific pattern. Therefore, the primitives required to build an ESN processing system are:

- Architectural topology of the reservoir
- Input and output processing layers
- Memristive synapse circuit models
- Neuron circuit models

This chapter introduces the circuits models used in this research. These models are used as building blocks for the proposed ESN architecture. They were designed by Mr. Cory Merkel, a Phd student in the NanoComputing research lab (RIT), in previous collaborated works [16, 39, 50].

3.1 Memristive Devices

Memristor is a two-terminal non-volatile variable resistor. It was first proposed in 1971 by Leon Chua [14] as a missing non-linear passive basic electrical component to be added to the three components resistor, capacitor, and inductor. Chua stated that there are six mathematical relations between the four fundamental circuit variables: voltage (v), current (i), charge (q), and flux (ϕ). Figure 3.1 shows these relations. The memristor relates electric charge $q(t)$ and magnetic flux linkage $\phi_m(t)$ equation 3.1.

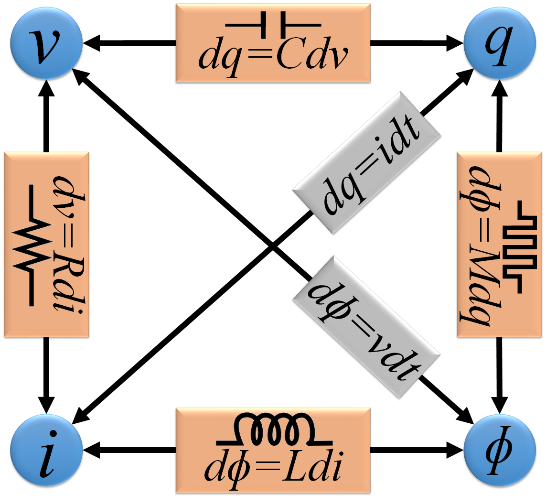

Figure 3.1: Relations between the four fundamental two-terminal circuit elements: resistor, inductor, capacitor, and memristor.

$$f(\phi_m(t), q(t)) = 0 \tag{3.1}$$

A memristor is characterized by its function that shows how the rate of change of charge and flux leakage depend on the state of the memristor [13] as shown in equation 3.2.

$$M(q) = \frac{d\phi_m}{dq} \tag{3.2}$$

Taking the time integral of this equation and substituting the flux as the time integral of the voltage and the charge as time integral of the current leaves us with resistance value as in equation 3.3. This equation shows that the resistance value of the memristor depends on the period of time and amount of current flow through the memristor.

$$M(q(t)) = \frac{V(t)}{(t)} \tag{3.3}$$

In 2008, Strukov *et al.* presented the first applicable memristor model using vacancy-doped titanium dioxide thin films [55]. Several other variations of memristor models have been presented. Each has diffenrent method to describe the memristive switching such as tunneling barrier modulation [43] and controlling the spin of electrons [41].

The resistance of memristor can be changed by applying voltage to its terminals. In the ideal memrsitor, any applied voltage should change the resistance. However in fabricated memristor models, the resistance is changed only when the applied voltage increases above a certain write threshold. Figure 3.2 shows the behavior of a piecewise memristor model vs voltage.

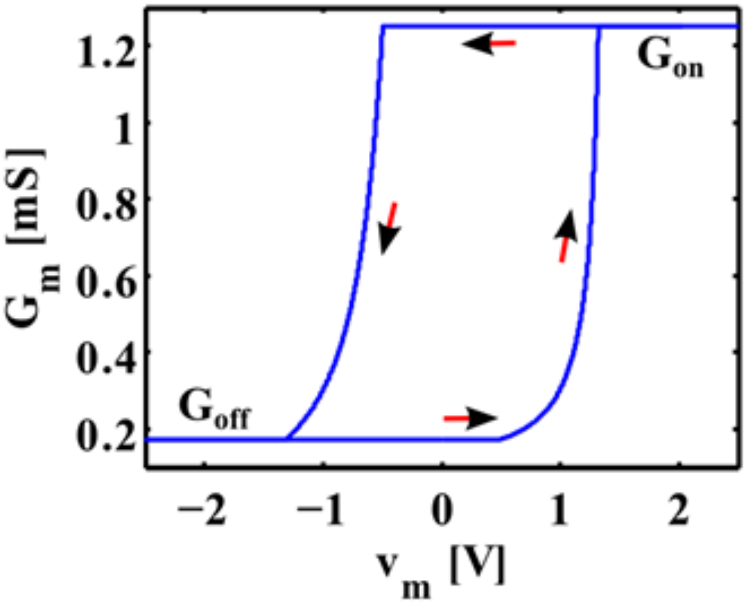

Figure 3.2: Charge vs voltage of a piecewise linear memristor model.

This figure shows that the charge linearly reacts to the voltage changes lower the write voltage. However, it dramatically changes ones the applied voltage increases above the write voltage. The write threshold divides the voltage scale of memristors into two regions: read and write. In the write region, the resistance of the memristor is changed to a desired value. The memristor retains this resistance state as long as no high voltage is applied. In the read region, the memristor acts as a linear resistor. This memory property is used to save synaptic weight values in synapse circuits [17, 44]. Memristors also have other attractive characteristics such as small footprint, simple device structure, and most importantly zero static power dissipation[30].

3.2 Synapse circuit models

Two synapse circuits are used in this work. The inhibitory synapse (Figure 3.3(a)) draws current away from a post-synaptic neuron, similar to GABAergic synapse in the biological brain. The excitatory synapse (Figure 3.3(b)) supplies current to the post-synaptic neuron, similar to glutamatergic synapse in the biological brain. In both the inhibitory and excitatory synapses, two memristors are used to save the weight value. Each memristor is connected to a diode connected transistor. The two memristors in parallel divide the input current based on the memristors conductance. Consequently the synaptic weight is given as a ratio of conductances as in equation 3.4.

$$w_{-(+)} = \frac{G_{2(4)}}{G_{1(3)} + G_{2(4)}} \tag{3.4}$$

where $G = 1/R$, is the conductance of memristors in figure 3.3.

The output current of the synapse circuits is driven through a current mirror, transistor $M3$ and $M6$ for the inhibitory and excitatory synapses respectively. The output currents inhibit or excite the post-synaptic neuron as shown in figure 3.3.

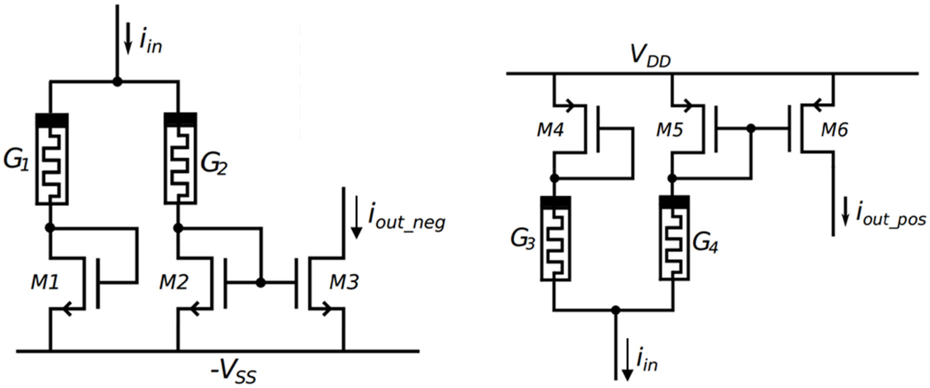

(a) (b)

Figure 3.3: (a) Inhibitory memristive synapse circuit and (b) excitatory memristive synapse circuit. These circuits are inspired by the function of biological inhibitory (*e.g.* GABAergic) and excitatory (*e.g.* glutamatergic) synapses with ionotropic receptors [39].

These circuits were originally designed based on bi-stable memristors where resistance values are assumed to be on one of the two extreme values, a high resistance state R_{off} and a low resistance state R_{on}. The combinations of these states give only five different weight values for both inhibitory and excitatory synapses. Figure 3.4 shows corner simulations of the circuits using only two memristor states. In this work the resistances of the memristors are extended to cover every possible state from R_{off} through R_{on}. This leads to high weight precision which gives high flexibility in simulation and improves the accuracy of the design.

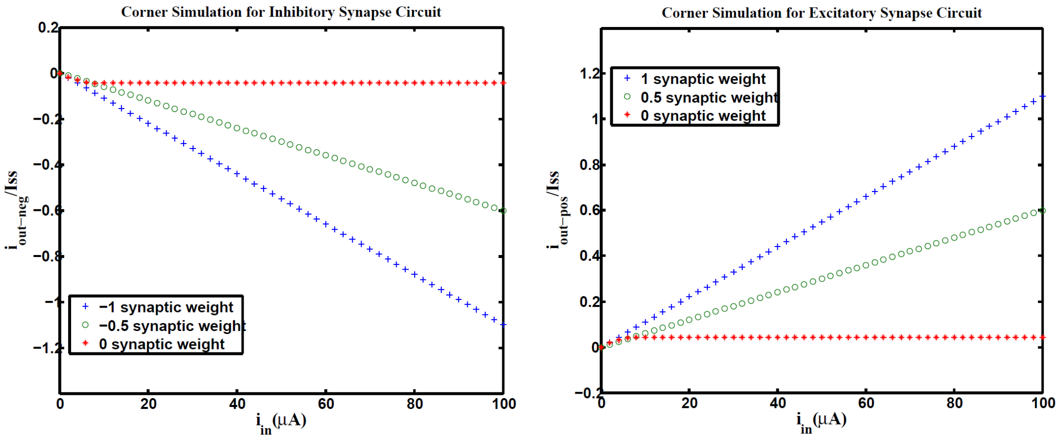

(a)

(b)

Figure 3.4: Corner simulation for (a) Inhibitory memristive synapse circuit and (b) excitatory memristive synapse circuit. Bi-stable memristors are used in these simulations under typical case (TT corner, 0.5V supply voltage, 27°C).

3.3 Neuron circuit models

A current-mode neuron circuit with a sigmoid activation function (Figure 3.5) is used in this work. This circuit consists of a MOSFET differential pair and a current mirror. The transistor $M2$ of the differential pair is grounded which makes the output current i_{out} depend only on the input current i_{in}. The output of the neuron normalized to maximum current, I_{max}, is described in equation 3.5. The input resistance R_{in} can be used to adjust the sigmoid slope. The maximum of i_{out} of the sigmoid function can be changed by tuning the transistor sizing of $M1$ and $M2$. The current flows in the differential pair is mirrored to the output through the transistor $M5$. Figure 3.6 shows simulation of the neuron circuit with input current i_{in}, which varies from $-10\mu A$ to $10\mu A$.

$$\frac{i_{out}}{I_{max}} \approx \begin{cases} 0 & , \mathrm{i}_{in} < -s \\ \frac{1}{2} - \sqrt{a} i_{in} R_{in} \sqrt{1 - a(i_{in} R_{in})^2} & , |\mathrm{i}_{in}| \leq s \\ 1 & , \mathrm{i}_{in} > s \end{cases} \tag{3.5}$$

where $a = \beta_n / 2I_{max}$, $s = \sqrt{2} V_{ov} / R_{in}$, and V_{ov} is the gate overdrive voltage defined as $V_{ov} = V_{GS} - V_t$.

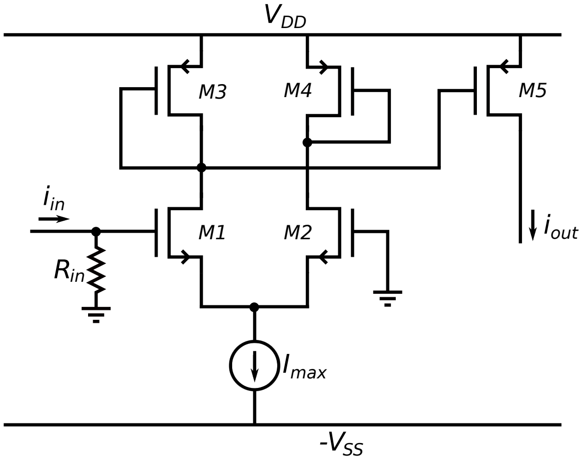

Figure 3.5: Neuron circuit for the reservoir layer of the ESN with a sigmoid activation function [39].

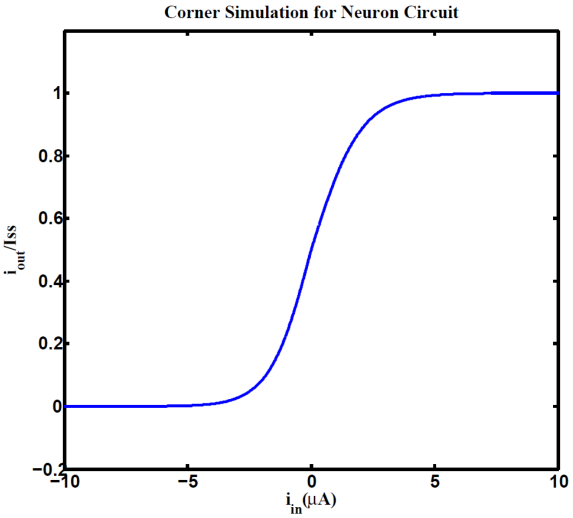

Figure 3.6: Simulation of the neuron circuit under typical case (TT corner, 0.5V supply voltage, 27°C). Input current i_{in} varies form $-10\mu A$ to $10\mu A$.

3.4 Summary

Memristor is a programmable resistor that changes its resistance based on its internal state. It has two voltages ranges: read and write. Applying write voltage updates the resistance while the read voltage has no effect on the resistance. Memristors are used as memory elements in synapse circuits. In this work two synapses, excitatory and inhibitory, are used. Each synapse uses two memristors to save weight values. The neuron circuits used in this architecture are composed of current-mode designs,which are inherently low power. These synapses and a current mode neuron circuit are used as building blocks for the proposed neuromemristive ESN architecture. The next chapter introduces this architecture.

Chapter 4

Proposed Topology and Architectures

4.1 ESN Topologies

Topology is defined as the interconnection pattern within the reservoir layer nodes. Several topologies for reservoir were presented in the literature [48]. This work particularly explores the random and ring topologies. It also presents a novel hybrid topology that minimize the required hardware resources.

4.1.1 Random Topology

The original ESN uses fully or randomly connected reservoir layer topologies [21]. The shape of these topologies and their degree of connectivity are defined by the reservoir layer weight matrix $\mathbf{W}_{\text{x}}$ where the weights of the unconnected links are set to zero. Such a random method to generate topologies for the reservoir layer has design constraints. It requires several trials to find the appropriate topology for an application. It is hard to regenerate these connections dynamically; it requires saving all the connections. There is no proofs that the generated pattern will be the best choice for the target application [48]. Moreover, the highly connected random topology is too complex to be implemented in hardware. The routing complexity, area overhead, and power consumption are significantly higher in hardware. For these reasons, simple reservoir topologies are desirable for hardware implementation of the ESN.

4.1.2 Ring Topology

The ring topology presented in [48] has a simple and hardware friendly structure. The nodes of the reservoir layer are connected in a ring shape where the output of each node is connected to only the neighboring node (Figure 4.1(a)). Equation 4.1 is used to calculate the state of a single node $x(s)$ in the reservoir layer at a certain time step n. This equation can be generalized to calculate the state of the entire reservoir layer as shown in equation 4.2.

$$\mathbf{x}(s)[n] = f^{\text{res}}(\mathbf{W}_{in}(s)\mathbf{U}[n] + \mathbf{W}_{ring}(s)\mathbf{x}(s-1)[n-1]) \tag{4.1}$$

where $\mathbf{x}(s)[n]$ is the state of node s at time step n. $\mathbf{W}_{in}(s)$ is the input weight associated with the node s. $\mathbf{U}[n]$ is the input at time step n. $\mathbf{W}_{ring}(s)$ is the reservoir weight between the nodes s and $s-1$. $\mathbf{x}(s-1)[n-1]$ is the state of the node $s-1$ at the previous time step $n-1$.

$$\mathbf{X}[n] = f^{\text{res}}(\mathbf{W}_{in}\mathbf{u}[n] + \mathbf{W}_{ring}\mathbf{X}\overset{\gg}{\underset{\ll}{[n-1]}}) \tag{4.2}$$

where $\mathbf{X}[n]$ is the state of all nodes in the reservoir layer at time step n. $\mathbf{W}_{in}$ is the input weights matrix. $\mathbf{W}_{ring}$ is the reservoir weight vector (one weight for each node). $\mathbf{X}\overset{\gg}{\underset{\ll}{[n-1]}}$ refers to the state of all nodes in the reservoir layer at time step $n-1$ rotated by one.

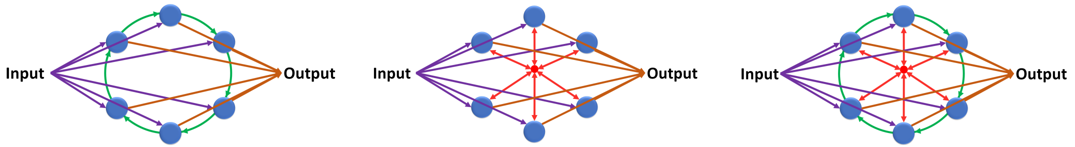

(a) Ring (b) Center Node (c) Hybrid

Figure 4.1: (a) ESN architecture with ring reservoir topology. Each reservoir node has 2 inputs and one output. (b) ESN architecture with center node topology. Reservoir nodes are connected to one center node that works as a hub. (c) ESN architecture with hybrid topology. Each node has 3 inputs and one output.

This topology provides low degree of connectivity in the network but has undesirable properties for the reservoir network. It has high network diameter and average distance. For a ring reservoir layer that has N number of nodes the diameter is $\mathbf{N-1}$ and the average distance is $\mathbf{\frac{2}{3}N}$. This means that the output effect of node $\mathbf{1}$ requires $\mathbf{N-1}$ time steps to reach the node $\mathbf{N}$. This high diameter may cause delay in the response of the reservoir to any changes in the input. Such delay is undesirable in real-time information processing applications.

4.1.3 Proposed Hybrid Topology

Simple updates to the ring topology can fix the high diameter and average distance values. Adding different shortcut links in the reservoir layer may decrease these values but it will make the network unbalanced, where the distance between the nodes will vary depending on its location from the shortcut links. Uniform connection links should be added to achieve constant distance between all nodes. Combining the ring topology, shown in figure 4.1(a), with the center node topology, shown in figure 4.1(b), may give the network the balanced uniformed shortcut links that increase the connections between nodes and improve network properties. Figure 4.1(c) shows the proposed hybrid reservoir topology. This topology has low diameter and average distance compared to the ring topology. The diameter is **2** and the average distance is less than **2**. In this way the reservoir is tightly connected and more sensitive to the changes to the input of the network. Equation 4.3 is used to calculate the state of the reservoir layer of the hybrid topology.

$$\mathbf{X}[n] = f^{\text{res}}(\mathbf{W}_{in}\mathbf{u}[n] + \mathbf{W}_{down}\mathbf{Xc} + \mathbf{W}_{ring}\mathbf{X}[n \underset{\ll}{\overset{\gg}{-}} 1]) \tag{4.3}$$

where $\mathbf{W}_{down}$ is the weight vector of synapses from the center node to the reservoir layer nodes. **Xc** is the state of the reservoir node. For further explanation, the mathematical derivation for the hybrid reservoir topology is shown in appendix A.

In terms of complexity, the hybrid topology has two extra synapses per node compared to the ring topology. These synapses connect the nodes of the reservoir layer with the center node. The idea behind using the center node is to provide each node in the reservoir layer with information about the state of the whole reservoir. It emulates the fully connected topology in which each node has full access to all nodes within the reservoir layer.

4.2 Proposed Architectures

4.2.1 Neuron Box

The neuron box is a container for the functional components in the ESN. Each neuron box contains one reservoir layer node and all the actively corelated synapses. These boxes are the building blocks of the proposed architectures that provide flexibility, reconfigurability and scalability.

In the ESN, there are three types of nodes: input layer nodes, reservoir layer nodes, and output layer nodes. These nodes are connected by three types of synapses: input layer to reservoir layer, reservoir layer synapses which connect the nodes within the reservoir layer, and reservoir layer to output layer synapses. In addition to these types, a few ESN models have additional types of synapses such as input layer to output layer synapses and feedback synapses from output layer back to reservoir layer. The ESN model in this work uses only the first three types of synapses. It can be noticed from the structure of the ESN that all three types of synapses are connected to the nodes in the reservoir layer, which represents a bridge between the input and the output layers.

The neuron box wraps one reservoir node and all the synapses that are connected to it in one frame. Figure 4.2 shows a neuron box for the ring topology ESN. As seen in this figure, the neuron box contains one neuron (reservoir layer node), one input synapse, one output synapse, and one reservoir synapse. The neuron box includes only input reservoir synapses. For this reason, there is only one reservoir synapse in the ring topology neuron box where the other synapse is included in the neuron box of the next node in the ring structure. The size of the neuron box depends on the number of synapses in the network and the size of the circuits of these synapses and the reservoir layer node. The neuron box does not includes the input nor output nodes because they are linear neurons and can be represented behaviorally.

Dividing an ESN into neuron boxes produce a number of homogeneous blocks that have the same number of ports, size, and structure. The number of these boxes is equal to the number of the reservoir layer nodes. Using neuron boxes simplifies the connectivity problem of the ESN. It can be thought of as a number of nodes (neuron boxes) that should be

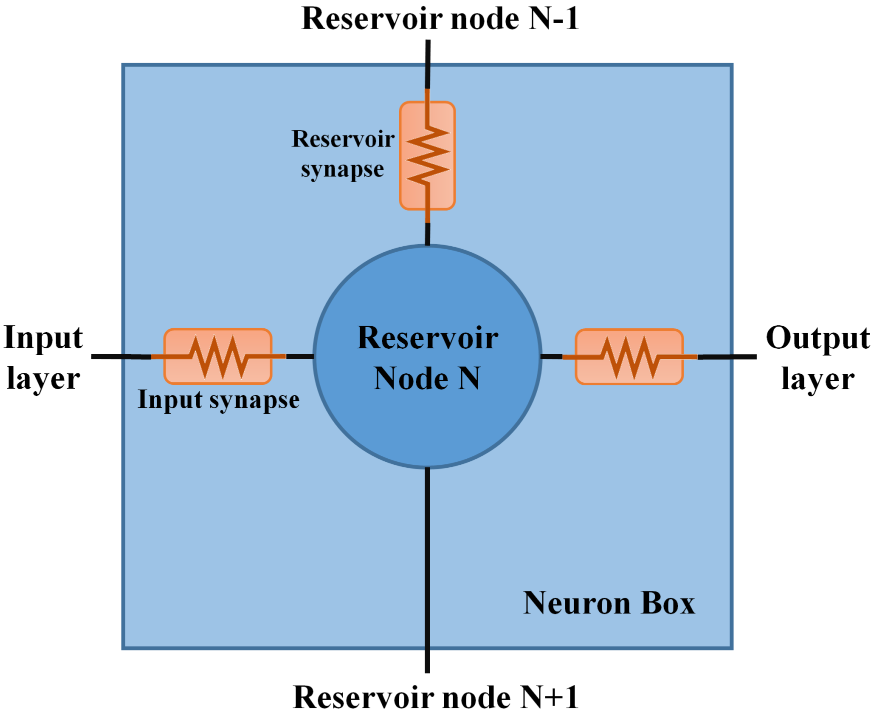

Figure 4.2: A neuron box of a ring topology ESN that has one input node and one output node. The neuron box contain one reservoir layer node, one input synapse, one output synapse, and one reservoir synapse connecting the reservoir layer node with the previous node.

connected according to a connection pattern. This makes the neuromemristive ESN architectures easier to implement, measure, and evaluate. Neuron boxes also provide scalability where a new neuron box is added to the architecture for each new reservoir node.

4.2.2 2-D Mesh Architecture for Ring and Random Topologies

In this work, hardware ESN model is built based on analog neuron and synapses circuits. These circuits are designed based on the assumption that they are always connected, which requires dedicated links to connect the circuits. This constraint is the main challenge for any proposed interconnect network. Moreover, the proposed architecture should have reconfigurability and scalability to implement several reservoir topologies with different sizes. These properties can be achieved with the neuron box and the appropriate interconnect network that has a flexible routing mechanism.

The proposed architecture uses 2-D mesh network topology to connect the neuron boxes. Similar network has been used for self-reconfigurable connectivity for FPGAs in [58]. A 2-D cellular automata is used where the routing between cells is decided by the cellular rules. The architecture proposed in this work is inspired by the network presented in [58]. In this architecture, each neuron box is connected to four neighboring boxes through full duplex links. The neighboring boxes are annotated north (N) south (S) east (E) west (W). This architecture allows any arbitrary connection between any two boxes in the network. Depending on the width of the links between the boxes, there could be some constraints to the possible connections. There are no constraints for the first connection, however, the more the connections added to the network, the more constraints are placed. The connection pattern between the neuron boxes is controlled by a set of multiplexers and switches that are added to each neuron box to form one cell in the 2-D mesh network. Figure 4.3 shows the internal architecture of one cell.

The states of these Mux's and switches are controlled by a memory register that is also included in the cell, where each cell requires seventeen bits. These bits are distributed between the Mux's (three bits for each Mux) and the switch which requires five bits. The connections between the cells are established according to the values of these bits which provide the required recofigurability to implement different ESN topologis. The registers of all cells in the network are serially connected. At the start-up time, the values of the bits are streamed to the registers. A bit file of the desired configuration for the entire network can be generated offline. This file is reusable for multiple implementations.

In the ESN model used in this work, the input layer and output layer are fully connected to the reservoir layer. These connections are never changed regardless of the ESN topology. An extra layer of cross-connectors are added to the 2-D mesh network to connect the input and output layers to the reservoir layer. Figure 4.4 shows a full ESN processing system that uses the proposed architecture. This figure shows an array of neuron boxes (blue balls) which form the heart of the architecture. The connections within the reservoir layer of the ESN are implemented using a 2-D mesh network through the routing switches (orange boxes) that are attached to the neuron boxes. The connections between the reservoir

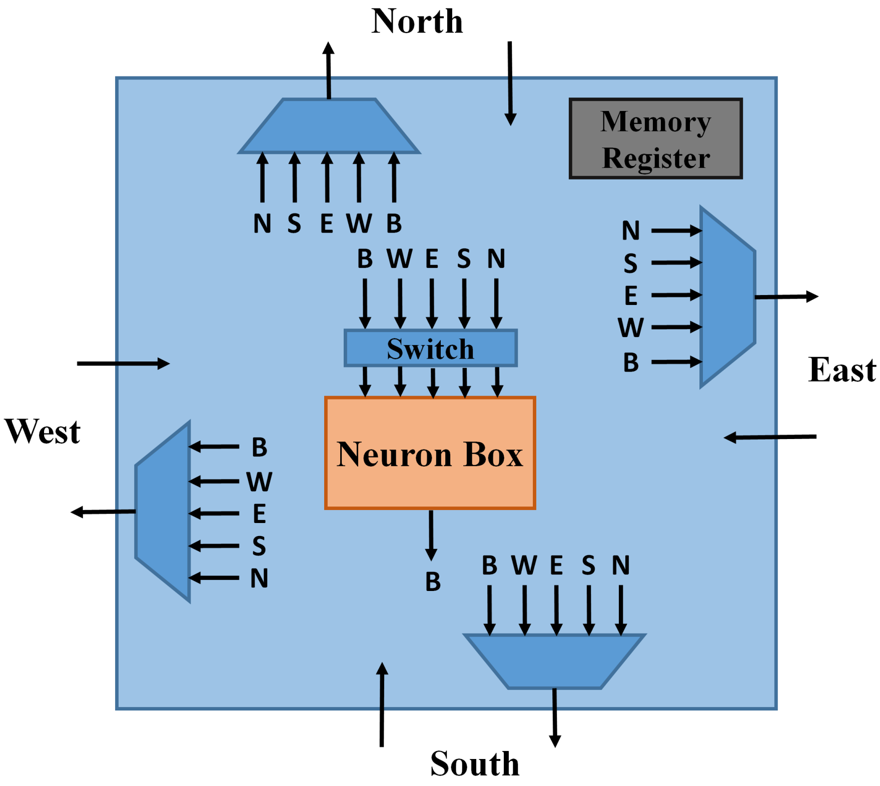

Figure 4.3: Internal structure of one cell. It contains one neuron box surrounded by four muxes and one four channel switch. These muxes and switches are used to control the routing of the links in the network.

layer and the input and output layers are implemented through the cross-connectors (green balls). The ESN system also contains pre-processing and post-processing steps. The pre-processing is the feature extractor while the post-processing is the circuitry used for the final output decision of the system. The post-processing could be a simple threshold circuit or a winner-take all circuit.

Two reservoir topologies were implemented using the 2-D mesh architecture: random and two way ring topologies. An example of the random topology is shown in figure 4.5(a). The two way ring topology, which is shown in figure 4.5(b), is a modified version of the ring topology that is discussed earlier in this chapter. It consists of two rings of connections. In this topology, node N in the reservoir layer has access to the outputs of both $N-1$ and $N+1$ nodes. The extra ring is used to increase the connectivity within the

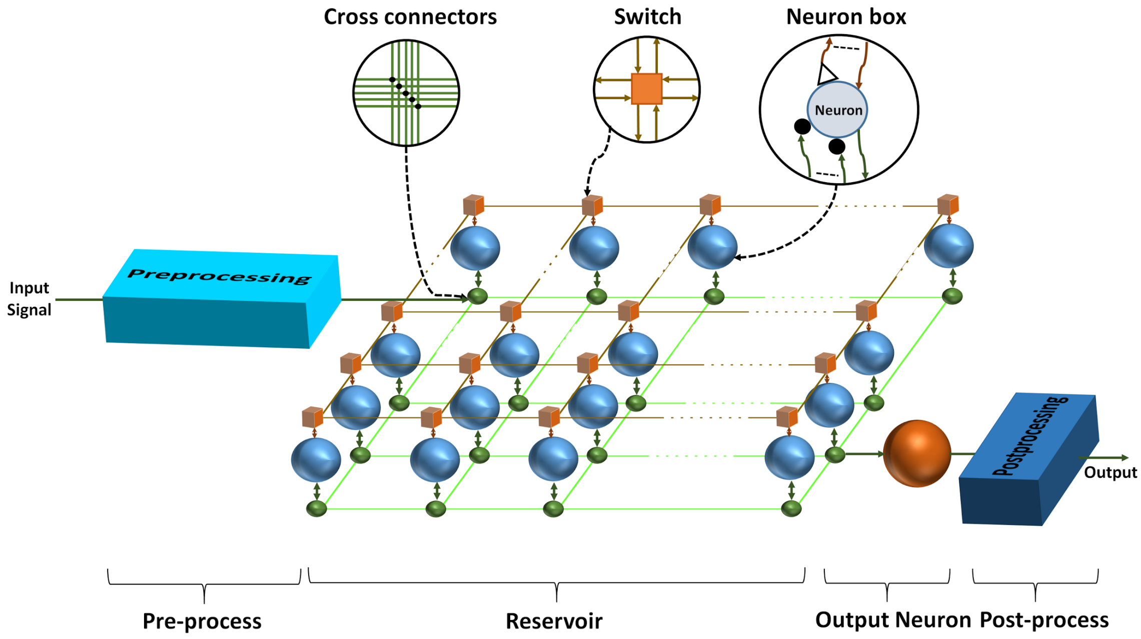

Figure 4.4: Complete system depiction of ESN architecture. The reservoir is implemented in 2-D mesh network with reconfigurable switches (colored orange) enabling dynamic configuration of different ESN topologies. The cross-connectors (colored green) are used to connect the input and output layers to the reservoir layer.

reservoir layer which impact the delay in the response of the ESN to the changes in the inputs. Figure 4.6 shows the implementation of the reservoir layers for these topologies on the 2-D mesh architecture. The random connections implemented on the 2-D mesh in figure 4.6(a) do not correspond to the random connections of the random topology in figure 4.5(a). The random and the two way ring topologies are used for speech emotion recognition and epileptic seizure detection applications respectively.

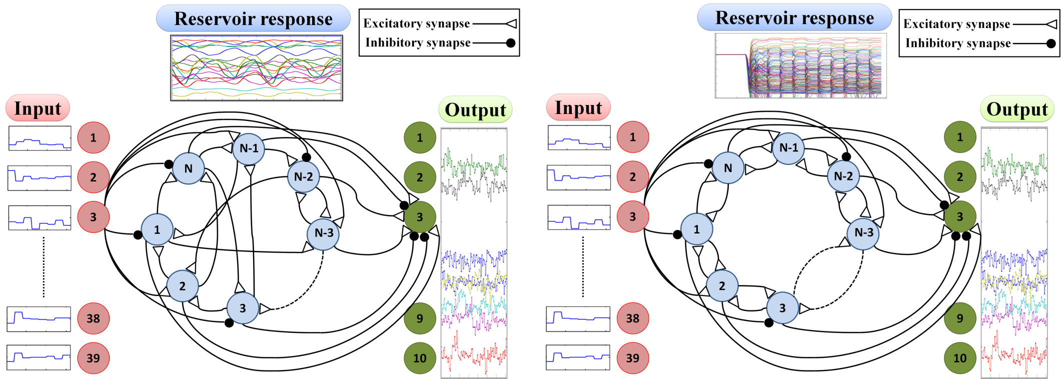

(a) (b)

Figure 4.5: Block level representations of the two ESN topologies. (a) Random topology and (b) Two way ring topology.

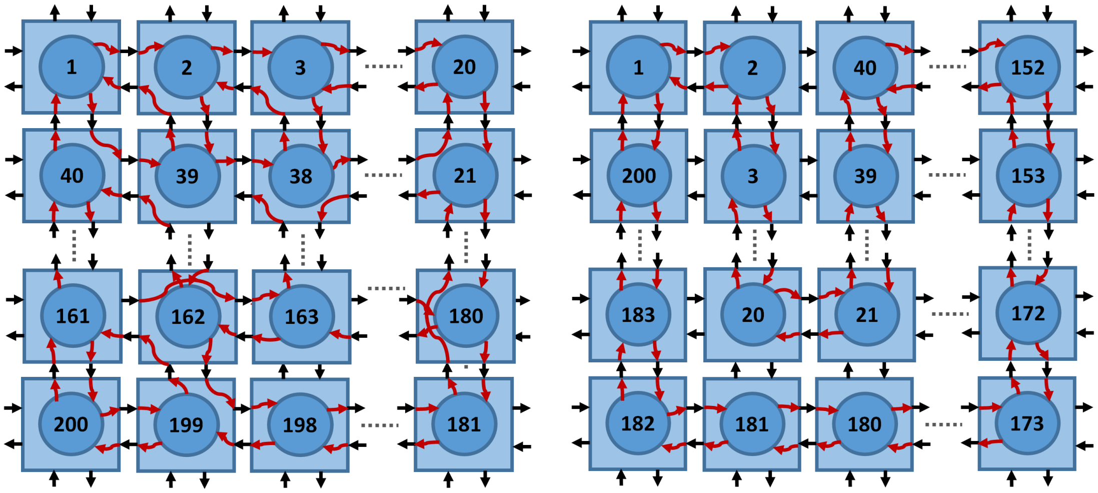

(a) (b)

Figure 4.6: Implementations of (a) Ring and (b) Random reservoir topologies on 2d-mesh network.

4.2.3 Toroidal Architecture for Hybrid Topology

The hybrid topology consists of four main groups of synaptic links: input set, output set, ring set, and center node set. The input and output synapses are fully connected to the reservoir. This means that the same signals are distributed for all nodes in the reservoir layer. One connection link that passes through all nodes in the reservoir layer in a ring shape can be used to distribute these signals. Since the center node is linear, which makes it a simple node that works according to Kirchhoff's current law, its connections can also be implemented as a ring (Figure 4.7). In this way, four rings can implement all the required connections of the hybrid topology as shown in figure 4.7. The rings in this figure are color coded to be consistent with figure 4.1(c) that shows the hybrid topology.

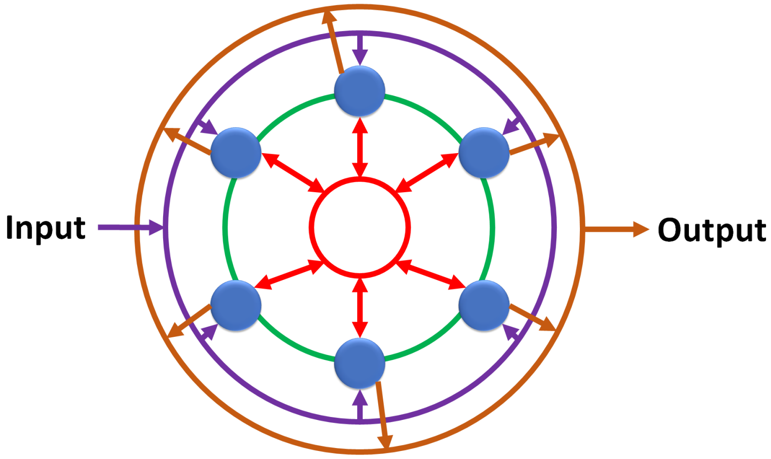

Figure 4.7: Implementing the hybrid topology as four rings. The rings are color codded based on figure 4.1. Purple ring is used for the connections between the input layer and the reservoir layer. Green ring is used for the ring topology connections. Red ring is used for the center node connections. Orange ring is used for the connections between the reservoir layer and the output layer.

Combining the neuron box with the ring connection patterns for the hybrid topology, produces a simple homogeneous architecture. With a suitable connection width, the 2-D mesh architecture can be used to implement the hybrid topology. However, using a reconfigurable architecture like the 2-D mesh for the static hybrid topology is inefficient utilization of the routing resources available in the 2-D mesh architecture. Instead, any static architecture that satisfies the four ring connections can be used.

In this work, the doubly twisted toroidal network is used to implement the hybrid topology. It has been used for several interconnection implementations. Martinez *et al.* [37] presented a modern modeling for twisted toroidal networks with the Gaussian integers. Beivide *et al.* [4] used twisted toroidal network for SIMD and MIMD architectures. Yang *et al.* [62] used a diagonal twisted toroidal network for massively parallel computer networks.

The doubly twisted toroidal network topology has the same array structure that traditional toroidal networks have with one extra connection for each row in the array. The idea is to add a ”twist” to the regular toroidal network. In the toroidal network, the opposite nodes at the beginning and end of each row and column are connected together while in the doubly twisted network, the last node at each row of the network is connected to the first node in the next row. The same twist connections are added in the vertical direction for the columns [53] [10]. Figure 4.8 shows an example of a doubly twisted network.

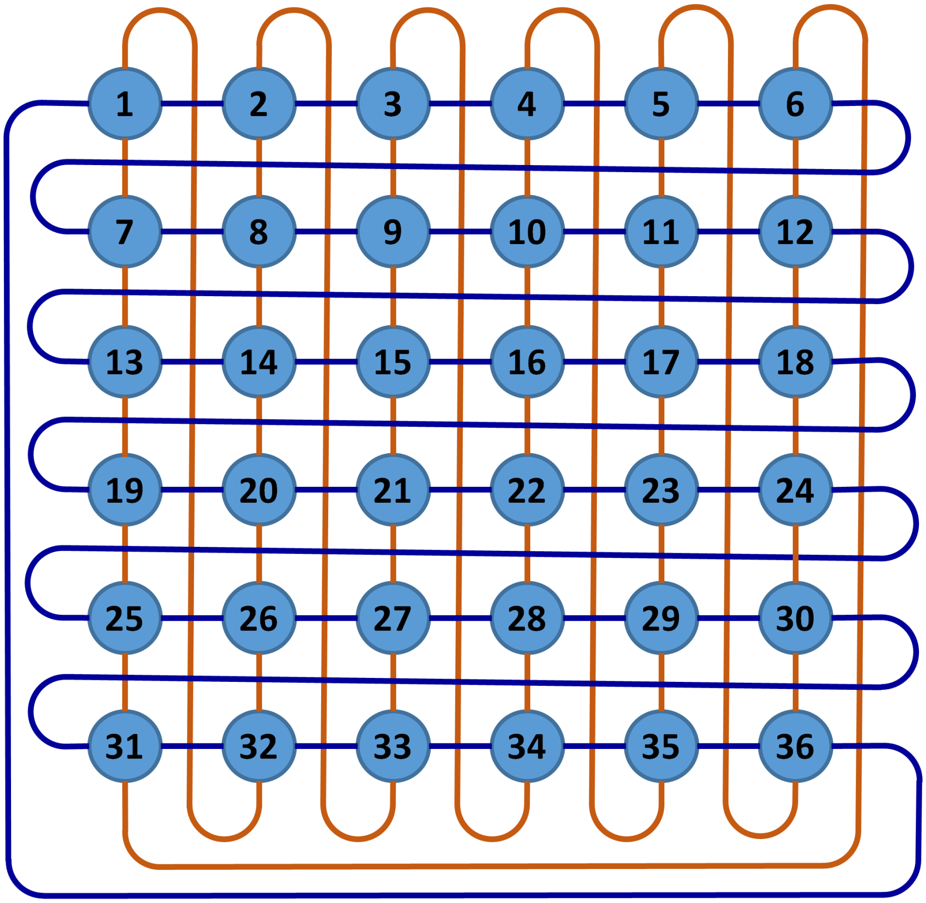

Figure 4.8: 6x6 doubly twisted toroidal network. The figure shows two rings connections are embedded in the architecture. One ring uses the horizontal links while the other uses the vertical links.

The nodes in the doubly twisted toroidal network represent neuron boxes of the hybrid topology. Four rings are required to connect these boxes. However, only two rings connections are embedded in the toroidal network as seen in figure 4.8. One ring uses the horizontal links while the other uses the vertical links. For this reason multichannel links are used in the doubly twisted toroidal network to increase the number of the embedded rings. This architecture is simple compared to the 2-D mesh architecture in term of the required resources, where no muxes, switches, or memory registers are used to route the signals. Consequently, it loses the reconfigurability property that the 2-D mesh has. On the other hand, scalability is still provided by the twisted toroidal architecture where any reservoir size can be implemented on this architecture.

4.3 Simulation Platform

The platform is the methodology used to simulate the proposed neuromemristive architectures. It consists of two parts MATLAB and HSPICE (Figure 4.9). A MATLAB script is used to generate HSPICE netlist for the synapses and neuron circuits. These netlists are simulated in HSPICE using 45 *nm* technology. The results are analyzed to build an ideal behavioral model of these circuits. Based on these models, the whole system was emulated in MATLAB, for a realistic simulation. The behavioral models are used to build an entire ESN system. The system includes managing the dataset, pre-processing (feature extractor), the neuromemristive reservoir architecture, and the post-processing. Three independent ESN systems are built for the three applications that are targeted in this work: epileptic seizure detection, speech emotion recognition and electromyography based finger recognition. Using this approach the systems are analyzed in detail to find the appropriate parameters to enhance the accuracy. The datasets and the feature extractors of the three applications are discussed in chapter 5 of this document. The results are presented and analyzed in chapter 6 of this document.

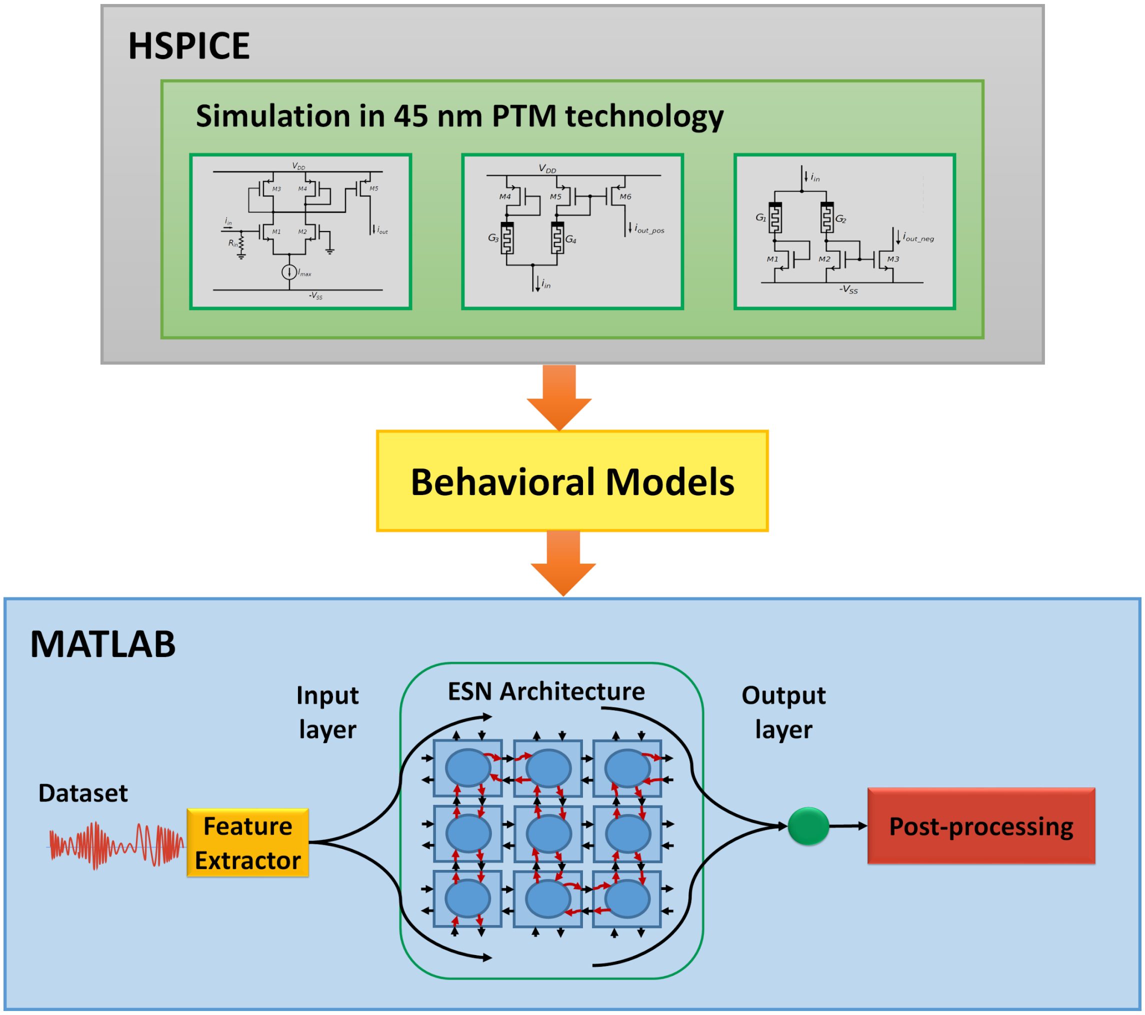

Figure 4.9: The simulation platform consists of two main parts: HSPICE and MATLAB. HSPICE is used to simulate the neuron and synapses circuits to build behavioral models. These models are used in MATLAB to build the neuromemristive reservoir architecture.

4.4 Summary

This chapter presents the proposed reservoir topology and the neuromemristive architectures. The hybrid topology is a combination of the ring topology and the center node topology. It has simple structure that has short diameter and average distance compared to the random and ring topologies. Two neuromemristive architectures are proposed: 2-D mesh and twisted toroidal architectures. Both of these architectures implement the ESN as a number of homogeneous neuron boxes. Each neuron box contain a reservoir node and the synapses associated with it. The 2-D mesh architecture uses muxes and switches to establish the connections between neuron boxes. This architecture has reconfigurability and scalability properties that gives the architecture the ability to implement different sizes and topologies of the ESN. The twisted toroidal architecture is used for the hybrid topology ESN.

Chapter 5

Benchmarks and Validation

5.1 Epileptic Seizure Detection

Epileptic seizure is a chronic disorder of the central nervous system. It is the fourth most common neurological disorder affecting 50 million people across the world [33]. Detecting epileptic seizures has several therapeutic applications, i) serves as an early alert system to preclude any unwanted exertion; ii) controlled delivery of drugs to reduce side effects; iii) continual monitoring for proactive intervention for anti-epileptic drug failures. Seizure, an aberration in the brain activity, can be often detected through analysis of electroencephalogram (EEG) signals. EEG signals are measured using surface or implanted electrodes in the tested region of the brain. The dataset used in this work is discussed in the next section.

5.1.1 EEG Dataset

The EEG dataset used was presented in [3]. It consists of 500 single-channel EEG segments of 23.6 sec. The dataset was divided into five sets (denoted A-E), each set contains 100 EEG segments. These segments were selected and cut form multichannel EEG records. Set A and E of this dataset are used in this work. Set A contains EEG recordings of five healthy volunteers in a relaxed state. Surface electrodes are used to collect the data in this set. The electrodes are placed according to a standardized electrode placement scheme as shown in figure 5.1(a). The signals were collected from all these electrodes where each segment contains data of one electrode. Set E contains seizure activity segments taken from five epilepsy patients during presurgical evaluation. Depth electrodes implanted symmetrically into the hippocampal formations of the brain were used to collect the data as shown in figure 5.1(b). Figures 5.2(a) and 5.2(b) show EEG signal samples of normal and seizure cases respectively. Signals in this dataset were recorded using the same 128-channel amplifier system. A 12 bit analog-to-digital converter is used to sample the signals at a rate of 173.61 Hz.

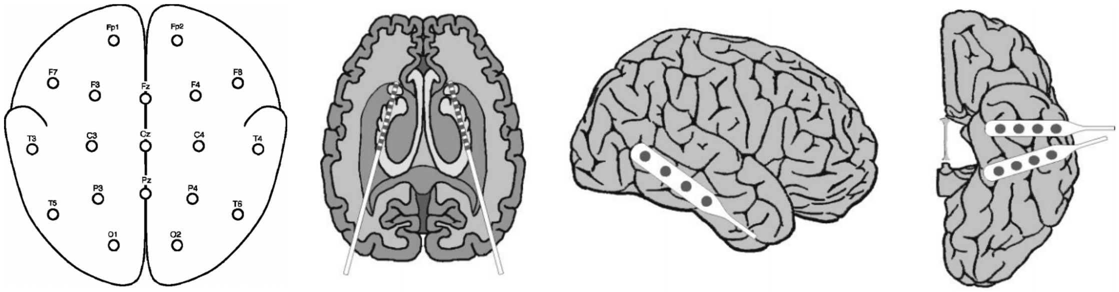

(a) (b)

Figure 5.1: Electrode placements as explained in [3]. (a) (the first white figure only) Standardized surface electrode placement scheme used to collect normal EEG signals of set A. (b) (three gray shaded figures) Scheme of electrodes implanted symmetrically into the hippocampal formation of the brain. This scheme was used to collect seizure EEG signals of set E.

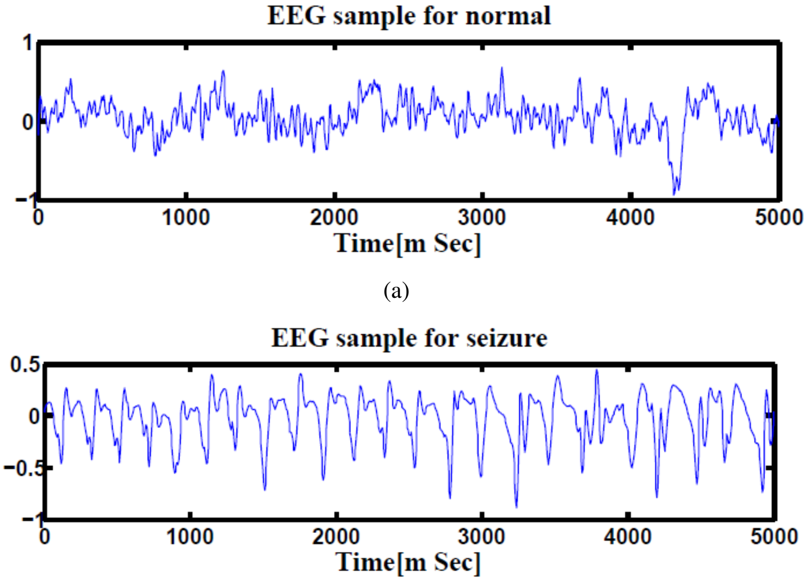

(a)

(b)

Figure 5.2: Five second time series EEG signal samples for (a) Normal case and (b) Seizure case.

5.1.2 Feature Extractor

Before feeding the input EEG signals into the ESN, desired features that contains information about seizures should be extracted. Four band pass filters are used as feature extractors in [9]. These filters cover the frequency range from 1 to 30 Hz. The output of these filters combined with the first derivative of the original EEG signals are used as feature candidates. A forward feature selection algorithm is used to choose some of these features. Continuous Wavelet Transform (CWT) formula is used to compose 16-channel EEG signals in [60]. This method is preferred over Fourier Transform because it can increase the frequency resolution in the frequency band of interest without affecting the time resolution. This work uses single channel EEG signals. A simplified feature extractor is considered. It normalizes input EEG segments and takes their absolute values. Such preprocessing step is desirable for hardware processing systems.

5.2 Emotion Recognition

With the advent of brain inspired computing systems, there is significant attention being given to speech emotion recognition. It is well-known that speech signals are the fastest and most effective method of communication among humans and believed to facilitate better human-computer interaction [15]. Speech emotion recognition will be particularly beneficial in applications where the response of the machine is based on the detected emotion, examples include therapeutic devices, autonomous driving systems, monitoring emotions in critical decision making environments, and personalized advertisements. Moreover using speech for emotion recognition requires fewer computational resources compared to other signals such as facial expressions. Based on the physiological studies it has been demonstrated that the sympathetic nervous system is stimulated with the expression of different emotions (joy, fear, and anger) and the parasympathetic nervous system is triggered for emotions such as sadness. The result is altered heart rate, blood pressure, respiratory movements, and muscle tremor, which in turn effect the energy, frequency, and pitch of the speech. It is also easier to collect the speech input signals compared to ECG/EKG signals or heart beat rate that require physical sensors. The tone of a persons voice changes over time as the words are uttered based on the emotional status. The emotional speech dataset used in this work is described in the next section.

5.2.1 Speech Emotion Dataset

The Berlin dataset of emotional speech is used for training and learning [6]. In this dataset, ten actors (five male and five female) recorded 800 utterances. Ten different daily used German sentences (5 short and 5 longer) are used in. These sentences are interpretable in all applied emotions and they contain no emotional bias. They were recorded in seven different emotional statuses (anger, sadness, fear, disgust, boredom, and neutral). The utterances were recorded in an anechoic chamber with high-quality recording equipment at 16 kHz sampling rate with 16 bit resolution.

5.2.2 Feature Extractor

Selection of features associated with emotions is an important step before feeding inputs into ESN. These features should be independent of the speaker or lexical content. In speech, emotion is communicated over varying temporal dynamics of the audio signal [51]. The human ear processes the tone, which contains the emotional information, as a non-linear function of the voice frequency. It linearly processes the frequencies below 1000 Hz; but its perception of frequencies more than 1000 Hz is logarithmic. To extract the emotion content as nearest as the human method, the Mel frequency scale is used [59]. The relation between Mel frequency and hertz frequency can be expressed by equation 5.1. Figure 5.3 shows a plot of this equation. As can be seen in this fgiure, the Mel scale loses its linearity on frequencies higher than 1000 Hz.

$$Mel(f) = 2595log(1+\frac{f}{700}) \tag{5.1}$$

Figure 5.4 shows a schematic representation of the feature extractor used in this work. The input audio signal $x(n)$ is divided into shorter pieces of 1600 samples. These pieces are overlapped with 640 samples. The Fast Fourier Transform $\mathbf{X}(k)$ of those vectors are

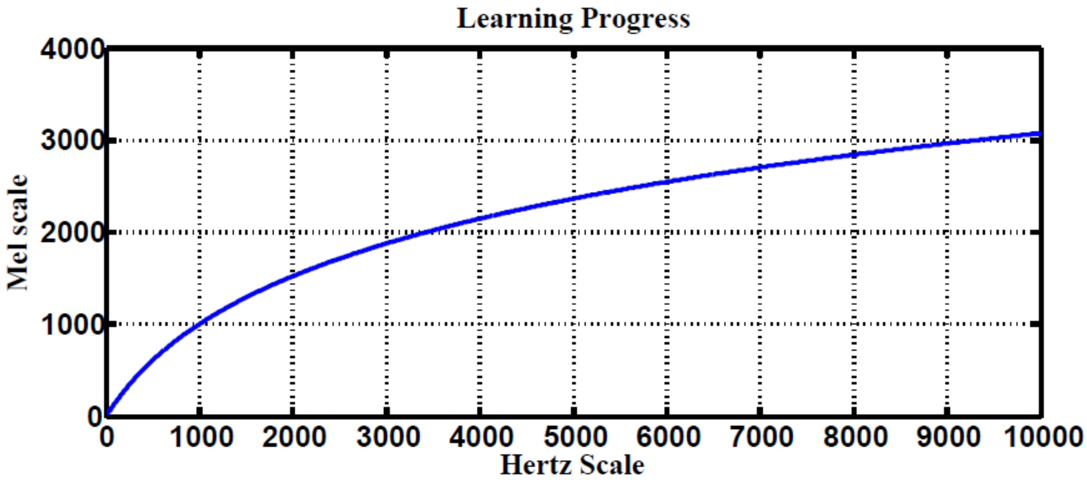

Figure 5.3: Mel scale generated using equation 5.1.

passed to eight triangular Mel-Filters. The limits of the filters are selected to mimic the human auditory system. The same frequency bands in [52] are used for the Mel-Filters in this work. Table 5.1 shows these bands. The frequency responses of these triangular filters are calculated based on equation 5.2.

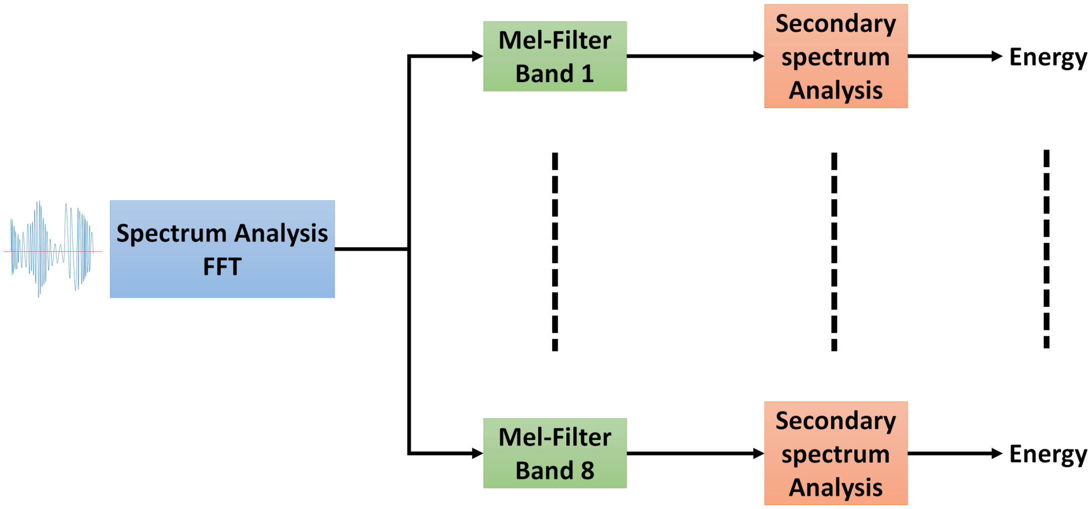

Figure 5.4: Block diagram of the feature extractor used in this work. The input is an audio signal and the final output is the energy corresponding to the emotion contents of the input signal.

Band	**Start Freq. (Hz)**	**End Freq. (Hz)**
1	32	578
2	257	964
3	578	1501
4	966	2217
5	1501	3180
6	2217	4433
7	3180	6972
8	4433	8256

Table 5.1: Frequency bands of Mel triangular filters. The start and end frequencies in this table represent b_i and d_i in equation 5.2 respectively.

$$\mathbf{H}_i[k] = \begin{cases} \frac{2(k-bi)}{(d_i-b_i)-(c_i-b_i)}, & \text{if } b_i \leq k \leq c_i \\ \frac{2(di-k)}{(d_i-b_i)-(d_i-c_i)}, & \text{if } c_i \leq k \leq d_i \\ 0, & \text{otherwise} \end{cases} \tag{5.2}$$

where i is the index of the filter, $\mathbf{H}_i$ is the frequency response of the i^{th} filter. b_i, c_i and d_i are the start, center and end limits of the i^{th} filter.

The amplitude spectrum of the signals analyzed by the Mel-Filter is calculated based on the responses of the frequency of the filter bands and the absolute value of the FFT $\mathbf{H}[k]$ (Equaion 5.3). This process ends with eight different signals and each signal is analyzed with FFT to calculate the final features. Based on the length and overlapped values of the input pieces, the extraction frequency is 25 Hz.

$$m(i) = \sum_{k=0}^{K} H_i[k]\,|X[k]| \tag{5.3}$$

Figure 5.5 shows the final features of ten neutral and ten anger statuses. It shows that the response of the third through eighth Mel-Filter bands for the neutral status is very low while the anger status shows high responses at these bands. This difference is the key to the classification.

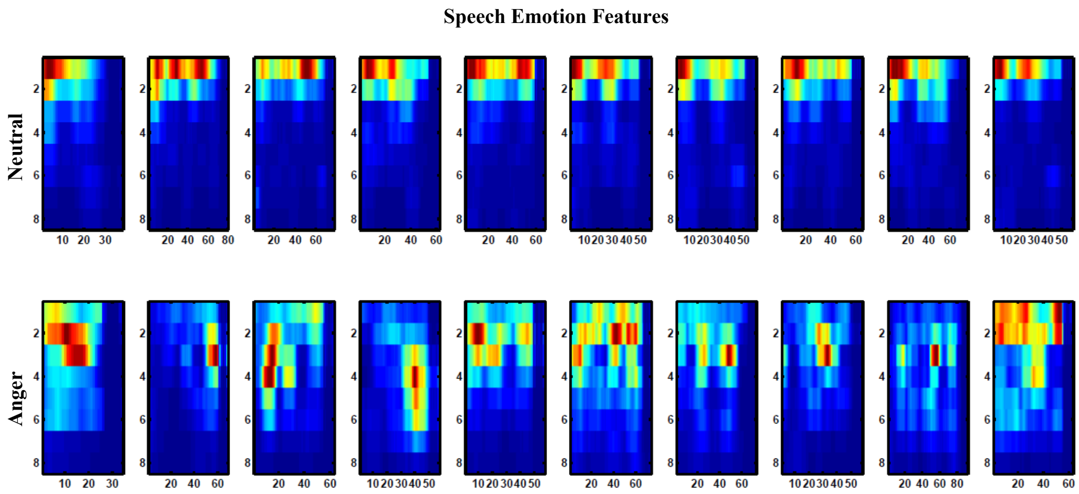

Figure 5.5: Ten randomly chosen final emotion features for neutral and anger statuses. The length of each of the signal depends on the length of the actual input audio signal to the feature extractor.

5.3 Electromyography

Electromyography (EMG) is a medical procedure to measure and record the action potential of the skeletal muscles which are neurologically or electrically stimulated [25]. EMG signals are measured by either needle electrodes injected into the muscles [28] or surface electrodes placed on the skin. The EMG contains information about the physical state of the neuromuscular system such as unit recruitment and firing and motion intention [26]. EMG has been applied in several medical applications such as diagnosing of neuromuscular diseases studying kinematic parameters and disorder of motor control [45]. It has also been applied to prosthetic device control and human computer interaction [61]. This work classifies EMG signals based on arm finger motion. The idea is to use the resulting information as input signals for prosthetic finger control.

5.3.1 EMG Dataset

The EMG dataset used in this project is presented in [27] with classification accuracy of 95%. It contains surface EMG signals recorded from six male and two female subjects aged between 20 and 35 years. These are healthy volunteers with no neurological or muscular disorders. The EMG signals were recorded while the subjects were moving their limbs and fingers according to a predefined procedure. Eight surface EMG electrodes were used to collect the data. The electrodes were placed across the circumference of the forearm as shown in figure 5.6(a). The signals were amplified to a total gain of 1000. They are sampled using 12-bits ADC at sampling rate of 4 kHz. The signals are band filtered between 20 and 450 Hz. The dataset is divided into 15 classes based on finger movements. It contains 3 EMG segments of each subject per class. Five classes representing individual finger movements are used in this project. Figure 5.6(b) shows these classes. The idea is to classify EMG signals based on finger motions. Figure 5.7 shows EMG signal samples of individual finger movements for the five classes used in this work.

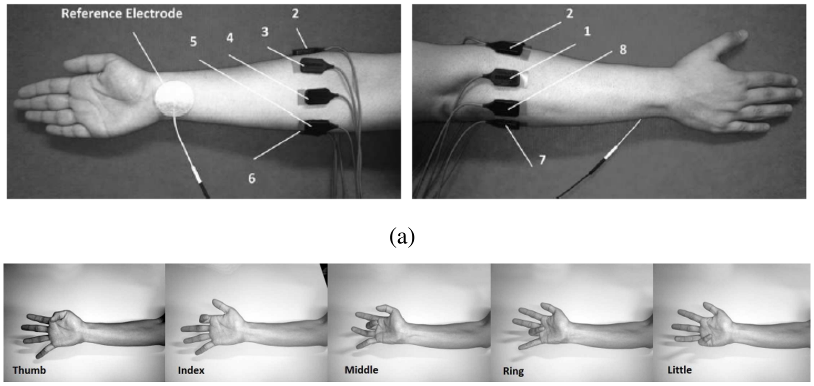

(a)

(b)

Figure 5.6: (a) Surface electrode placement on the forearm. (b) Five classes of individual finger movements used in this work [27].

5.3.2 Feature Extractor

Different feature extractors have been used in EMG signal analysis. Two step feature extractor is used in [27], the first step is mutual information evaluation function, which reduces the uncertainty of one random variable, given information of another random variable. The output of this function is projected on principle components analysis (PCA). Zhang *et al.* [63] used sampling entropy (SampEN) analysis for detecting onset muscles activity. SampEn is a modified version of approximate entropy introduced in 2000 by Richamn and Moorman [47]. It measures the complexity and randomness of physiological time-series signals independently from length of data segment under test. Pinymork *et al.*

[42] used fifty time and frequency domains features to classify ten upper limb motions. Results showed that SampEn has the best accuracy compared to other features that were investigated such as ApEn waveform length (WL), root mean square (RMS), and cepstral coefficients (CC). This work uses SampEn analysis as feature extractor of EMG before feeding signals to the ESN. The input EMG segments are divided into short windows of length 250 *ms* with 125 *ms* intervals. The same parameters for SampEn in [42] are used in this work. The Matlab code for SampEn is developed by Kijoon Lee [31].

5.4 Summary

Three bio-signal benchmarks are used to test the proposed architecture. The EEG signals are used for epileptic seizures detection, which has several medical applications. The speech emotion recognition is mainly useful for applications that require human computer interaction. The EMG signals are used to test electrical activity of skeletal muscles. In this work EMG signals are used for motion detection. The datasets of these benchmarks and their feature extractors are described in this chapter. Next chapter presents the results obtained from applying these signals onto the proposed neuromemristive reservoir architecture.

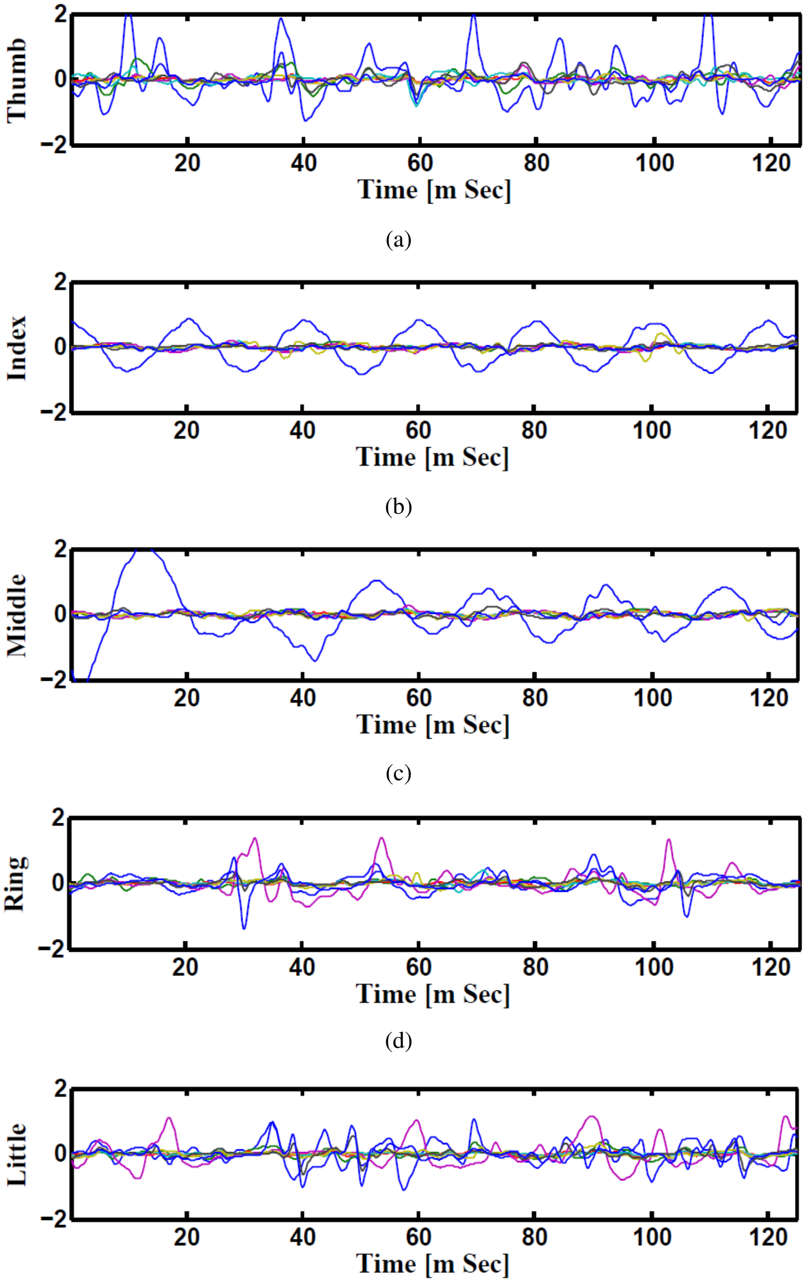

(a)

(b)

(c)

(d)

(e)

Figure 5.7: EMG signal samples of individual finger movements for (a) Thumb, (b) Index, (c) Middle, (d) Ring, and (e) Little.

Chapter 6

Results and Performance Analysis

6.1 Applications

6.1.1 Epileptic Seizure Detection

Two hundred EEG segments (160 for training and 40 for testing) are used for epileptic seizure detection. The normalized absolute values of these segments are fed into the ESN. The output of the ESN is compared against a threshold value to calculate the final binary output.

Two ESN topologies are used for epileptic seizure detection: ring topology and hybrid topology. Several simulations were conducted for each topology to find the best reservoir size and alpha value that give the highest classification accuracy. Figure 6.1(b) shows the testing accuracy vs reservoir size and alpha for the rign and random topologies. In the two topologies, the accuracy increases as the reservoir size increases. However, the accuracy stabilizes within a range once the reservoir size exceeds 100 nodes. Changing alpha value does not have as much affect on the accuracy. In general, alpha value of 0.5 works for the two topologies. The maximum accuracy achieved is $\approx$86% and $\approx$90% for the ring and hybrid topology respectively. The extra synaptic connection within the reservoir layer is behind this increase in the accuracy. These connections increase the interaction between reservoir nodes and provide more information about the overall situation of the reservoir to each node which increases the response of the reservoir to the changes in the input.

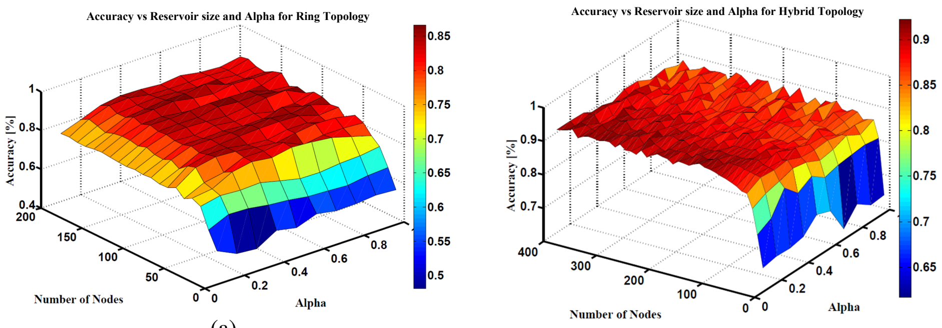

(a)

(b)

Figure 6.1: Epileptic seizure detection accuracy versus the reservoir size and alpha for (a) Ring topology with maximum accuracy of 86% and (b) Hybrid topology with maximum accuracy of 90%.

6.1.2 Emotion Recognition

Two emotional statuses are tested in this work: anger and neutral. The restricted analysis of two emotional statuses was chosen to simplify hardware testing and reservoir parameters optimization. The dataset and feature extractor used for emotion recognition are discussed in chapter 5. A total of 156 audio signals were used for both training and testing purposes (110 for training and 46 for testing). The random topology is used for the emotion recognition. Repeated sets of simulations were conducted to find the best values of the size of the reservoir, degree of connectivity and the short memory parameter alpha. 1000 individual simulation runs were conducted with different reservoir sizes (10-500) and degrees of connectivity ($5-100\%$). Figure 6.2 shows the testing accuracy of each simulation. It was found that the 190 node reservoir with 20% degree of connectivity has the best accuracy. These values were used to conduct another experiment to find the best Alpha value. The experiment included 100 distinct simulation runs with different Alpha values (0.01-1.0). Figure 6.3 shows results of this experiment where the best testing accuracy was achieved when Alpha value $\approx$0.25.

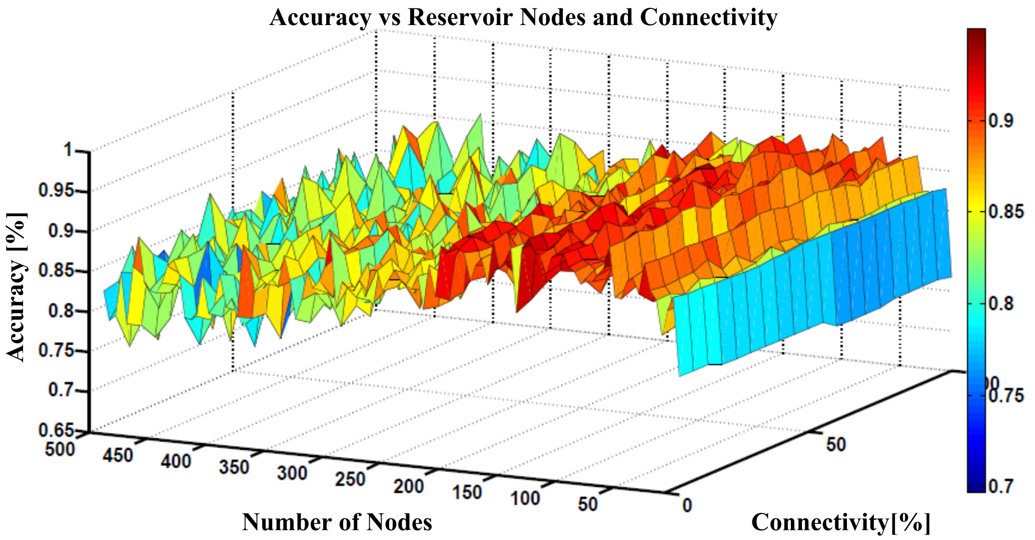

Figure 6.2: The effects of the number of nodes within the reservoir and the degree of connectivity of those nodes on the testing accuracy at Alpha ≈0.25. The best accuracy is observed at ≈190 nodes and ≈ 20% connectivity.

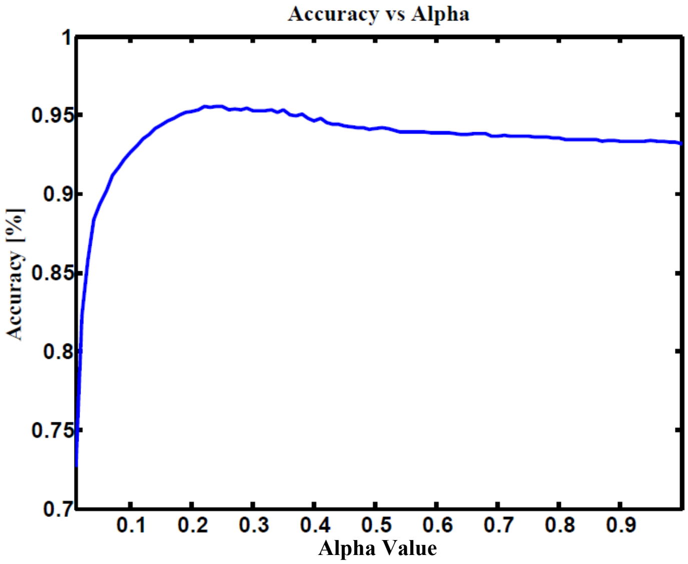

Figure 6.3: The short memory parameter Alpha verses testing accuracy at 190 reservoir nodes with 20% connectivity. Best accuracy is observed at Alpha ≈0.25.

One readout layer node was sufficient to classify the two emotional status (Neutral and Anger). The output of this node is compared against a threshold value to calculate the final binary output. Figure 6.4 show the expected output, actual output vs threshold value, and predicted output. Different threshold values were used to enhance the classification accuracy. Figure 6.5 shows best training and testing accuracy versus different threshold values. Both training and testing reached ≈96% accuracy.

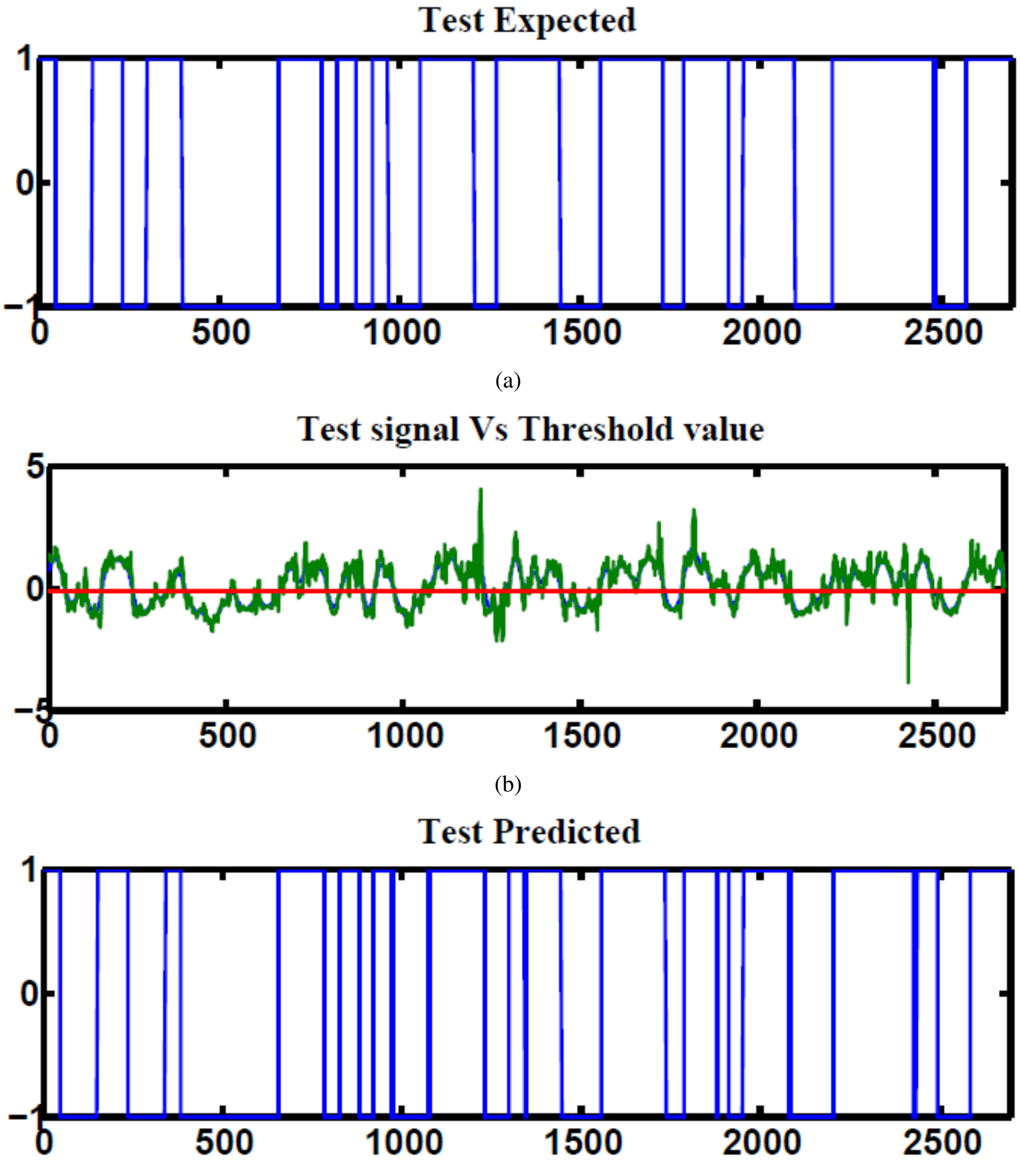

(a)

(b)

(c)

Figure 6.4: Signal propagation through ESN for speech emotion recognition at (a) Test expected, output signal Vs threshold, and test predicted.

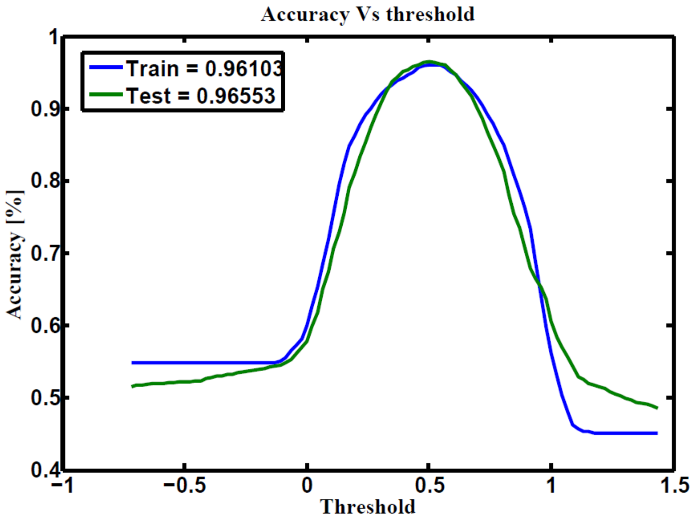

Figure 6.5: The classification accuracy of ideal hardware behavior model of the ESN with 190 reservoir nodes at 20% degree of connectivity and Alpha ≈0.25 The best test accuracy is 96.5%.

6.1.3 Prosthetic Fingers Control

Five classes of individual finger motions are used in this work. The dataset and feature extractor used for this application are discussed in chapter 5. Each class contains 24 EMG segments of length 20 seconds. The segments are divided into smaller parts of length 4 seconds. This will increase the total number of segments to 120 per class. 100 segments are used for training while the rest 20 segments are used for testing. The hybrid ESN topology is used for finger motion classification. Eight input nodes are used (one node for each EMG channel) while five nodes are used for the output (one node per class). The output signals of these nodes are processed using winner-take all method to calculate the final binary output. The performance of the hybrid topology was analyzed to find the best parametric values. Several simulations were conducted over varied reservoir size and alpha values. Figure 6.6 shows the test accuracy vs reservoir size and alpha. The average accuracy of ten trials for each combination of size and alpha is showed in this figure. The accuracy increase as the size of the reservoir increase for the sizes lower than 300 nodes. However, the accuracy stabilizes in a range for the larger reservoir sizes. The maximum training and testing accuracy achieved is 87% and 84% respectively. Figure 6.7 shows confusion matrices of classification accuracy of training and testing.

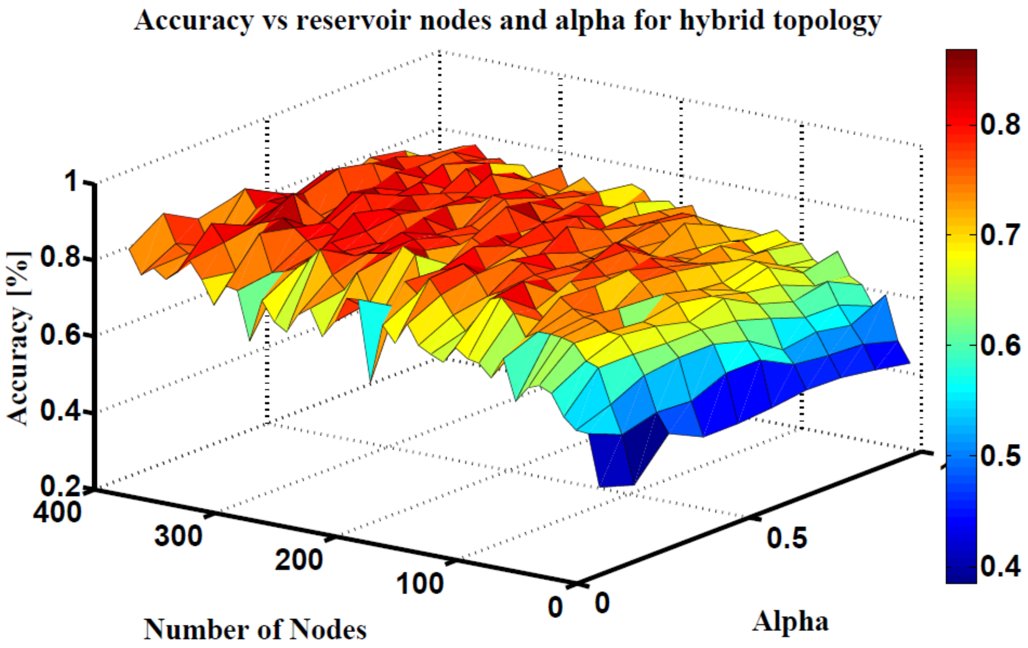

Figure 6.6: The effects of the number of nodes within the reservoir and alpha on the testing accuracy of finger motion recognition using hybrid topology.

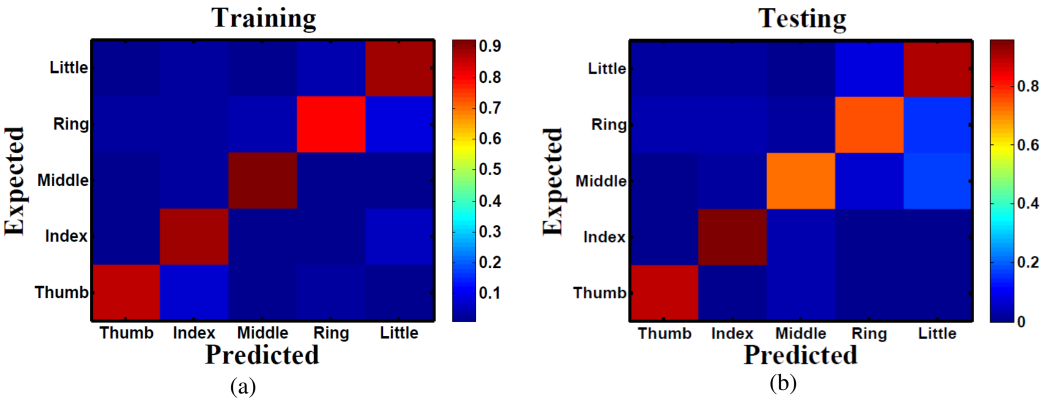

(a)

(b)

Figure 6.7: Confusion matrix of fingers classification from surface EMG signals using 300 nodes hybrid reservoir for (a) training with accuracy of 87% and (b) testing with accuracy of 84%.

Some applications of human computer interaction may require recognition of one finger motion. For instance, a signal that can be used to control an on/off button. In such application, the classification problem is simplified; instead of recognizing which exact finger is moving, this application test for movement of a specific finger. The idea is to answer the question: is finger X is moving or not? regardless of the situation of other fingers. This can be implemented using different post processing step. Instead of winner-take all, a threshold comparator can be used for each output node. In this application the accuracy increase to a range from 88% to 95%. Figure 6.8 shows the classification accuracy vs different threshold value for the five classes. Each class has different threshold value that gives the maximum accuracy.

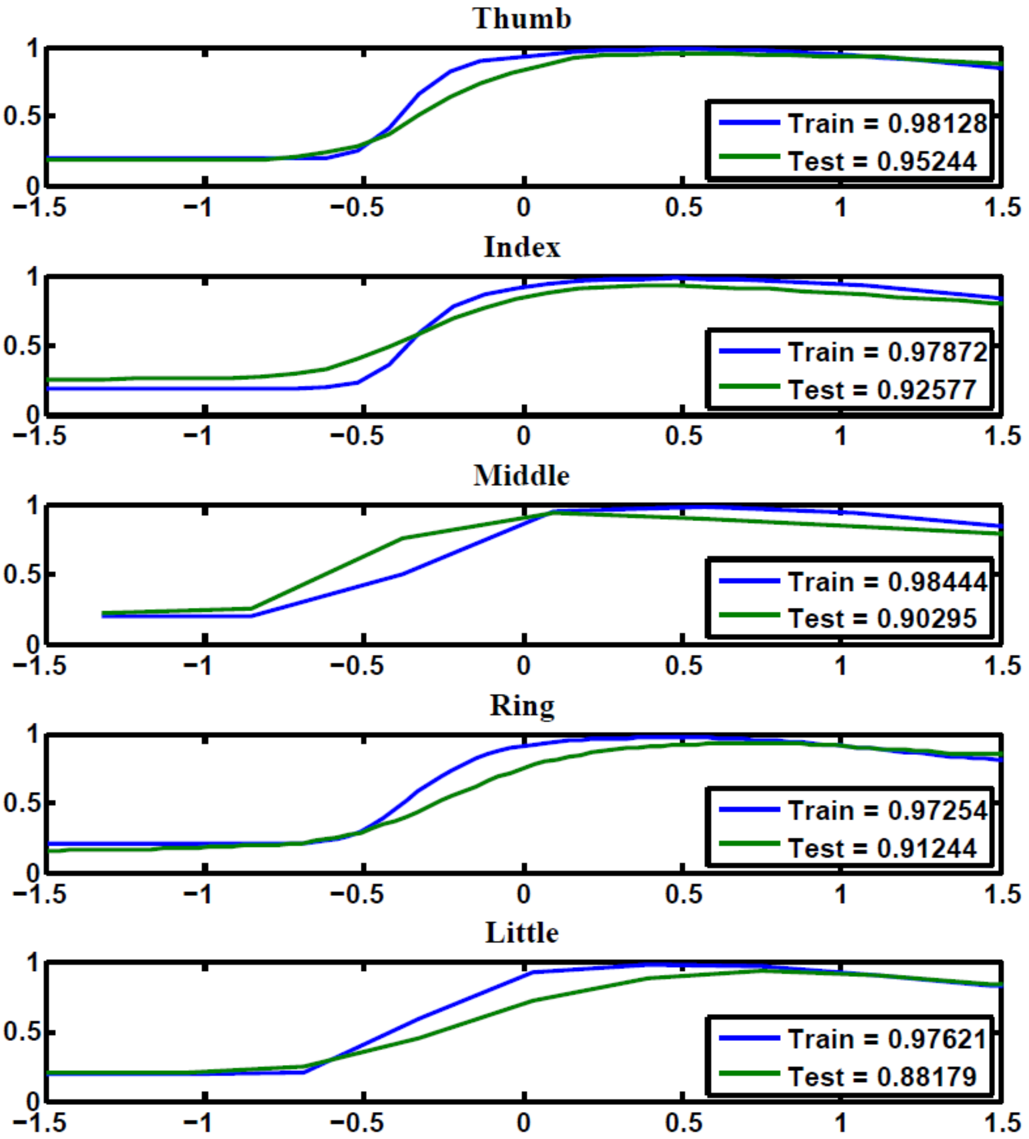

Figure 6.8: Classification accuracy of individual finger motion. The accuracy is in a range from 88% to 95%.

6.2 Reservoir Metrics

The performance of the reservoir is dependent on the randomly generated weights of the reservoir and several other parameters such as alpha and reservoir size. Finding the best values for these parameters has been an open question. The over all performance of the reservoir has been used to study effect of these parameters. This requires a complete training of the reservoir for a specific application, which takes long time and requires more processing resources. Further more the best parameter values may vary depending on the targeted application. More general metrics that are independent from the target output are required to test the reservoir. These reservoir metrics are measurements of the quality of the reservoir. Several metrics have been proposed in the literature [40, 18]. Chrol-Cannon *et al.* [12] compared the ability of four reservoir metrics to measure the performance of several reservoir topologies. The reservoir metrics used in this study are: class separation, kernel quality, Lyapunove's exponent, and spectral radius. Results showed that kernel quality and Lyapunove's exponent strongly correlate with reservoir performance. These two metrics are used in this work for the hybrid topology while processing two types of data: EEG and EMG. They are used to study the effect of reservoir size on the quality of the reservoir. The test is implemented over varied reservoir sizes 10 to 100 node. To study the stabilization of these metrics hundred trials are used for each size.

6.2.1 Kernel quality

Kernel quality is a measure of linear separation property of the reservoir. It is first presented in [32] and proposed by Chrol-Cannon *et al.* [12] as a reservoir metric. The reservoir response to the whole set of input vectors is used to calculate this metric. The whole reservoir states are concatenated in a matrix M where each column in M represents reservoir response to one input vector. The kernel quality is calculated by taking the rank of this matrix. It represents the network freedom to represent each input stimulus differently. The target kernel value is equal to the size of the reservoir which means that each reservoir node generate its unique response that can't be regenerated by using linear combinations of the responses of the other nodes.

Figure 6.9 shows kernel quality results for the hybrid reservoir topology processing EEG and EMG signals. The median of kernel quality values are close to the target for different reservoir sizes for both EEG and EMG signals. Results also showed that there is variation of the kernel quality values especially for reservoir sizes larger than 50 node. This variation is a result of the randomly generated weight for the input and reservoir synapse where low kernel quality value could be a result of unsuitable set of random weights. In general the kernel quality value for EMG data seems more stable compared to those of EEG data. The nature of the input signals could be behind this small difference between the EEG and EMG.

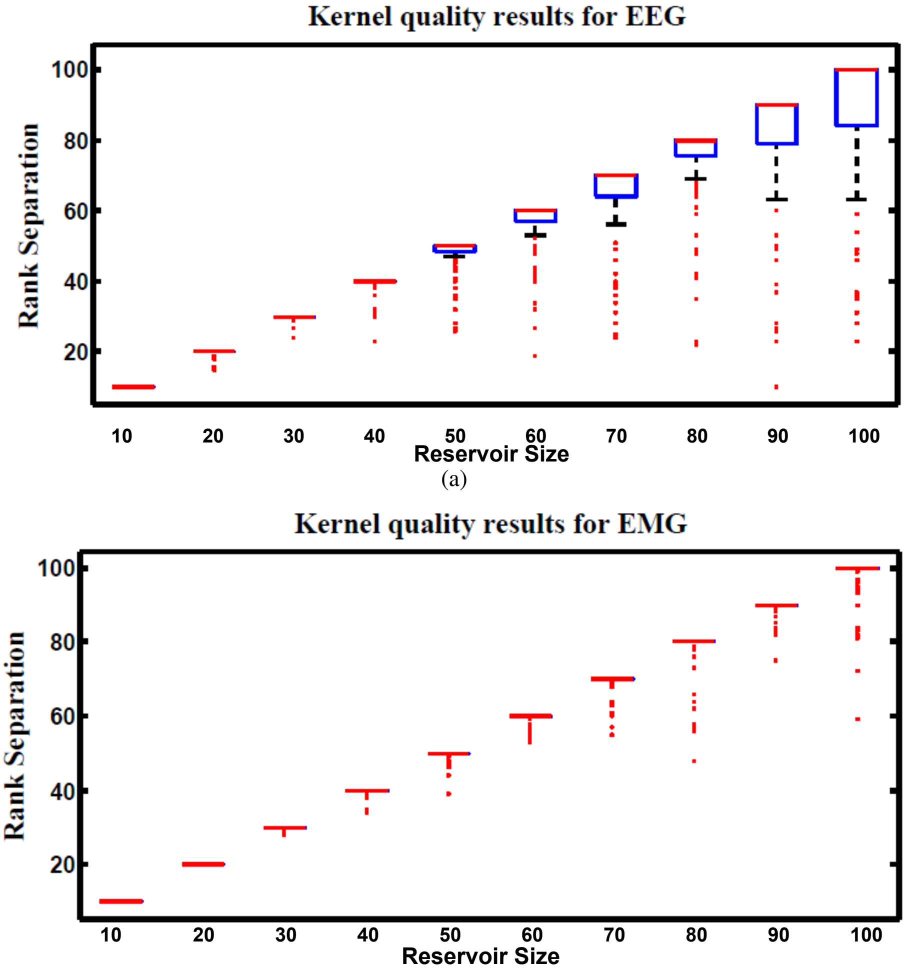

(a)

(b)

Figure 6.9: Kernel results vs different reservoir sizes for hybrid topology reservoir testing (a) EEG and (b) EMG signals.

6.2.2 Lyapunov's Exponent

Lyapunov's exponent is a measure of the chaos in the dynamic response of the reservoir. This metric was formulated in [18]. Equation 6.1 is used to calculate Lyapunov's exponent value. Positive values of this metric represent the chaotic dynamic region while negative values represent the stable region. Since the optimal reservoir performance occurs at the edge of chaos, Lyapunove's exponent of zero is desirable.

$$\lambda(t) = k \sum_{n=1}^{N} \ln \left(\frac{\left\| x_j(t) - x_{\hat{j}}(t) \right\|}{\left\| u_j(t) - u_{\hat{j}}(t) \right\|} \right) \tag{6.1}$$

where $u_j(t)$ is an input to the reservoir at time step t. $u_{\hat{j}}(t)$ is the nearest neighbor to $u_j(t)$. $x_j(t)$ and $x_{\hat{j}}(t)$ are the reservoir response to $u_j(t)$ and $u_{\hat{j}}(t)$ respectively.

Figure 6.10 shows Lyapunov's exponent results for the hybrid reservoir topology processing EEG and EMG signals. Results showed that the values of this metric are higher than zero for EEG signals while it showed that they are around zero for EMG signals. This means that the hybrid topology has more chaotic response to the EEG signals compared to the response of the EMG signals. It also showed that the size of the reservoir processing the EEG signals has low effect on the value of Lyaponv's exponent compared to the reservoir processing the EMG signals. As in kernel quality, there is variation in the values of Lyapunov's exponent and this is also attributed to the random weights of the input and reservoir synapses.

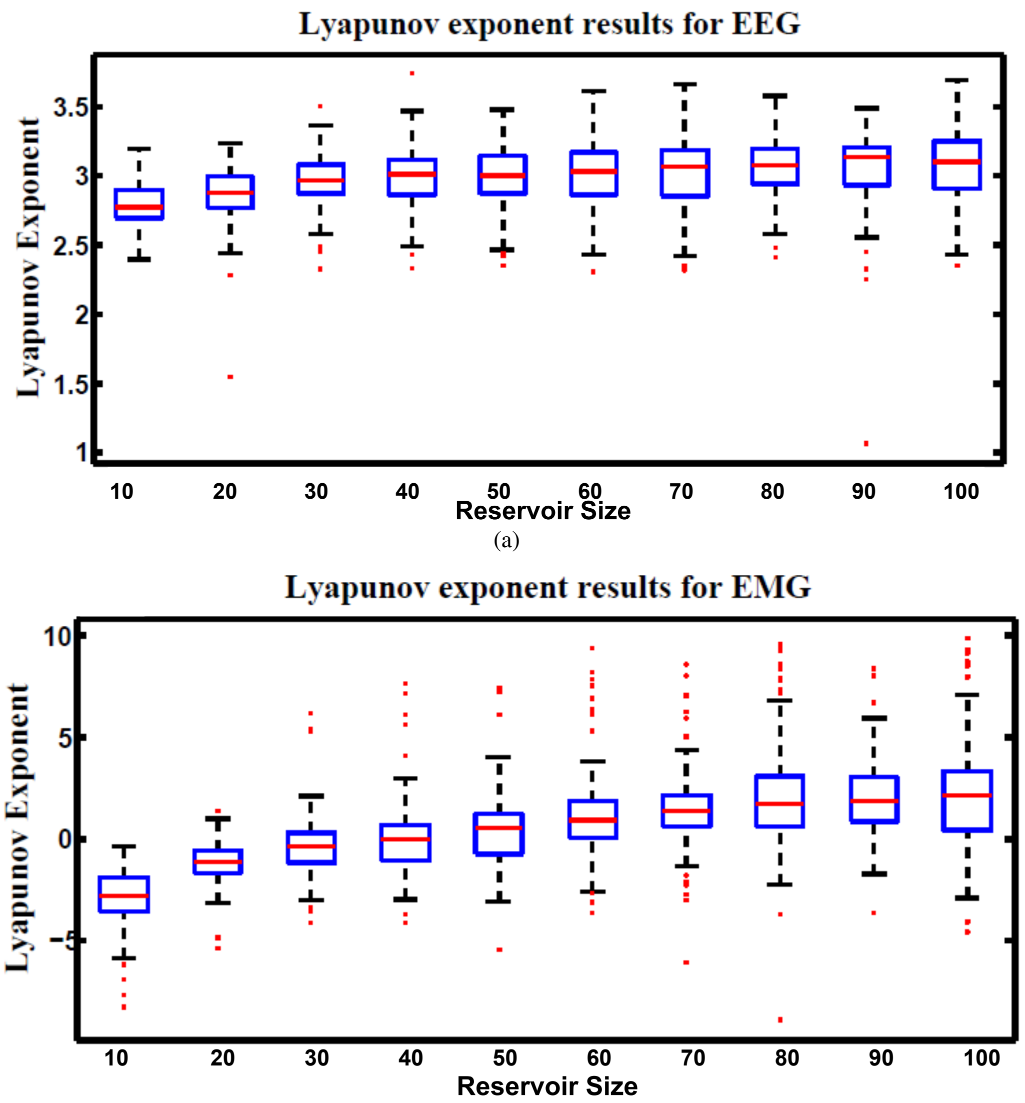

(a)

(b)

Figure 6.10: Lyapunov's exponent results vs different reservoir sizes for hybrid topology reservoir testing (a) EEG and (b) EMG signals.

6.3 Power

Power dissipation of four different reservoir topologies is analyzed. The average dynamic power dissipation is measured in HSPICE for small size reservoirs. The maximum current I_{max} used in the simulation is $10\mu A$. These measurements are quantitatively scaled for larger reservoir sizes. Figure 6.11 shows the power dissipation of three reservoir topologies, one way ring, two way ring, and hybrid, over different reservoir sizes. The power dissipation of the three topologies is in tens mile watts. Results showed that the one way ring topology has lower power consumption compared to the two way ring and hybrid topologies. This is attributed to the small number of synapses that the one way ring topology has where each reservoir layer node has only one synapse. Results also showed that the relation between power dissipation of these topologies and reservoir size is linear. This implies that there is no power dissipation overhead for increasing the size of the reservoir. Figure 6.12 shows the power results for four reservoir topologies: one way ring, two way ring, hybrid and random. The random topology has higher power dissipation (in order of several watts) because it has high number of synapses compared to the other topologies. It also showed that the power dissipation of the random topology is exponentially related to the size of the reservoir. For this reason the random topology is not desired for the hardware implementation. The power consumption of these topologies can be reduced using subthreshold designs and other power reduction techniques.

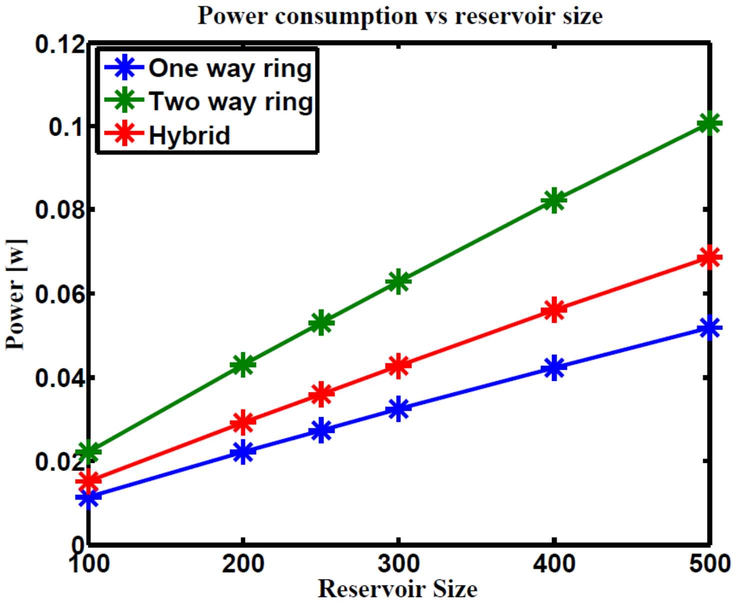

Figure 6.11: Power consumption vs reservoir size of three ESN topologies: one way ring, two way ring, and hybrid. The ring topology has lower power consumption compared to the other topologies.

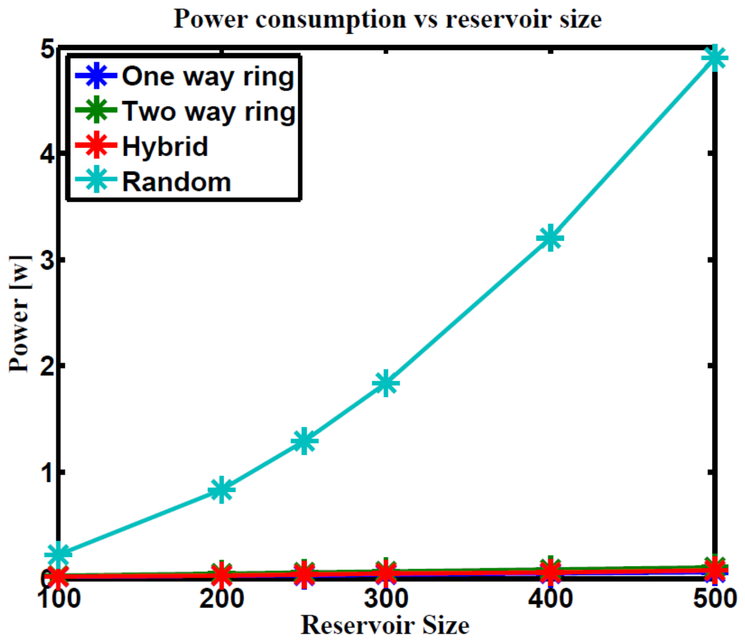

Figure 6.12: Power consumption vs reservoir size of four ESN topologies: one way ring, two way ring, hybrid, and random. The random topology has higher power consumption compared to the other topologies.

6.4 Summary

Three reservoir topologies, ring, hybrid, and random are used for the three applications implemented in this work. The ring and hybrid topologies are used for epileptic seizure detection. The maximum accuracy achieved using the ring and hybrid reservoir topologies is 86% and 90% respectively. The random topology is used for the emotion recognition with accuracy of 96%. The hybrid topology is used for prosthetics finger control with accuracy of 84%. Reservoir quality is analyzed for the hybrid topology using two reservoir metrics: kernel quality and Lyapunov's exponent. Results showed that the hybrid topology has more stable response to the EMG signals compared to the response to the EEG signals. The power dissipation of different reservoir topologies is also analyzed. Results showed that the one way ring topology has lower power consumption compared to the other topologies. It also showed that the random topology has very high power consumption which makes it undesirable topology for hardware implementation.

Chapter 7

Conclusions and Future Work

7.1 Conclusions

This thesis work proposed a neuromemristive ESN architecture. ESN is a recurrent neural network that has simplified training algorithm. It has been applied to several spatiotemporal recognition problems. The untrained recurrent connections within the ESN are used as filter for extraction of features in the temporal domain. The output of this filter is used to train the output layer of the ESN using linear regression. The proposed ESN neurmemristive architecture is useful for power constrained devices. Mixed-signal circuits have high design cost, but are the prime choice for realizing ESNs. The proposed architecture uses the 2-D mesh network and doubly twisted toroidal network as interconnection platforms. Several ESN topologies are implemented on the proposed architecture. The work also proposed a hybrid ESN topology that has low number of synapses and high connectivity. The choice between the ESN topologies is determined by the accuracy of the the target application, input data stream, and hardware resource availability.

Three medical and human computer interaction applications are used to test the proposed architecture. The architecture achieved an accuracy of 90%, 96%, and 84% for epileptic seizure detection, speech emotion recognition and prosthetic fingers control. The quality of the ESN is analyzed using kernel quality and Lyapunov's exponent metrics. The power consumption of different ESN topologies is also analyzed. The power dissipation of the one way ring, two way ring, and hybrid topology is in tens mile watts. The random topology has higher power consumption compared to the ring and hybrid topologies. In general, for the applications tested in this work ESN performance is comparable to the state-of-the-art.

7.2 Future Work

The architecture proposed in this work can be used for applications in other therapeutic systems and body sensors such as diagnose of neuromuscular disease, analysis of ECG/EKG signals, and prediction of epileptic seizures. Such power constrained devices are on the top of list of applications that can benefits from the neuromemristive architectures. Furthermore, the applications used in this work can be expanded. For instance, more emotional statuses can be used in the speech emotion recognition instead of only two statuses. Combined finger motions can be added to the prosthetic finger control. Other ESN topologies can be explored to increase the accuracy of the system and reduce hardware requirements.

Training circuitry for the memristors can be incorporated in this system. Such circuits can be used for on chip training. To reduce the power consumption of the architecture, other synapse and neuron circuit models can be used. These new circuit models can directly replace the current circuits where the proposed architecture is not constrained to specific circuits. Subthreshold designs and other power reduction techniques are also a suggested to reduce the power consumption. The proposed architecture can be expanded for other types of reservoirs such as liquid state machine.

Appendix A

Derivation for Hybrid Topology

A.1 is the traditional equation to calculate the state of the reservoir

$$\mathbf{X}(n+1) = f^{\text{res}}\left(\mathbf{W}_{\text{in}}\mathbf{u}[n+1] + \mathbf{W}_{\text{x}}\mathbf{x}[n]\right) \tag{A.1}$$

The second part of this equation $\mathbf{W}_{\text{x}}\mathbf{x}(n)$ represents the interconnections within the reservoir layer. This part can be used to calculate the state of the reservoir layer independently from the input layer. In other words, if there are R nodes in the reservoir layer, this part can be modified to calculate the state of one node in the reservoir layer $\mathbf{x}(s)$ as shown in equation A.2. For derivation purposes, equation A.2 neglects the reservoir activation function f^{res} and the input to the network $\mathbf{u}$.

$$\mathbf{x}(s) = \sum_{r=1}^{R} \mathbf{W}_{\text{x}}(s)(r)\mathbf{x}(r) \tag{A.2}$$

$\mathbf{W}_{\text{x}}$ in equation A.2 can be divided into two groups: $\mathbf{W1}_{\text{x}}$ and $\mathbf{W2}_{\text{x}}$. As shown in equation A.3.

$$\mathbf{x}(s) = \sum_{r=1}^{R} \mathbf{W1}_{\text{x}}(s)\mathbf{W2}_{\text{x}}(r)\mathbf{x}(r) \tag{A.3}$$

$$\Rightarrow \mathbf{x}(s) = \mathbf{W1}_{\text{x}}(s)\sum_{r=1}^{R} \mathbf{W2}_{\text{x}}(r)\mathbf{x}(r) \tag{A.4}$$

A.4 can be divided into two parts as shown in equation A.5 and A.6.

$$\mathbf{Xc} = \sum_{r}^{R} \mathbf{W2}_{\text{x}}(r)\mathbf{x}(r) \tag{A.5}$$

$$\mathbf{x}(s) = \mathbf{W1}_{\mathrm{x}}(s)\mathbf{Xc} \tag{A.6}$$

Equation A.5 is used to calculate the state of the center node **Xc**. This node is fully connected to all nodes in the reservoir layer. Based on **Xc** the state at one node $\mathbf{x}(s)$ in the reservoir layer can be calculated as shown in equation A.6. For convenience $\mathbf{W1}_x$ and $\mathbf{W2}_x$ are named $\mathbf{W}_{down}$ and $\mathbf{W}_{up}$ respectively.

$$\Rightarrow \mathbf{Xc} = \sum_{r}^{R} \mathbf{W}_{up}(r)\mathbf{x}(r) \tag{A.7}$$

$$\Rightarrow \mathbf{x}(s) = \mathbf{W}_{down}(s)\mathbf{Xc} \tag{A.8}$$

These two equations A.7 and A.8 are used in to calculate the state of the reservoir layer of the center node topology. Combining these equations with the equation of the ring topology gives the equation for the hybrid topology as shown in equation A.9.

$$\mathbf{x}(s) = \mathbf{W}_{down}(s)\mathbf{Xc} + \mathbf{W}_{ring}(s)\mathbf{x}(s-1) \tag{A.9}$$

Equation A.9 can be generalized to calculate the state of all nodes in the reservoir layer of the hybrid topology as shown equation A.10. This equation considers the input to the network and the reservoir activation function.

$$\mathbf{X}[n] = f^{\mathrm{res}}(\mathbf{W}_{in}\mathbf{u}[n] + \mathbf{W}_{down}\mathbf{Xc} + \mathbf{W}_{ring}\mathbf{X}[\overset{\gg}{\underset{\ll}{n-1}}]) \tag{A.10}$$

Bibliography

[1] An introduction to epilepsy. http://www.epilepsy.com/.

[2] Towards intelligent computing with neuromemristive circuits and systems, 2014.

[3] Ralph G. Andrzejak, Klaus Lehnertz, Florian Mormann, Christoph Rieke, Peter David, and Christian E. Elger. Indications of nonlinear deterministic and finite-dimensional structures in time series of brain electrical activity: Dependence on recording region and brain state. *Phys. Rev. E*, 64:061907, Nov 2001.

[4] Ramon Beivide, Enrique Herrada, Jose L Balcazar, and Jesus Labarta. Optimized mesh-connected networks for simd and mimd architectures. In *Proceedings of the 14th annual international symposium on Computer architecture*, pages 163–170. ACM, 1987.

[5] J. Burger and C. Teuscher. Variation-tolerant computing with memristive reservoirs. In *Nanoscale Architectures (NANOARCH), 2013 IEEE/ACM International Symposium on*, pages 1–6, July 2013.

[6] Felix Burkhardt, Astrid Paeschke, Miriam Rolfes, Walter F Sendlmeier, and Benjamin Weiss. A database of german emotional speech. In *Interspeech*, volume 5, pages 1517–1520, 2005.

[7] Lars Büsing, Benjamin Schrauwen, and Robert Legenstein. Connectivity, dynamics, and memory in reservoir computing with binary and analog neurons. *Neural computation*, 22(5):1272–1311, 2010.

[8] Pieter Buteneers, Benjamin Schrauwen, David Verstraeten, and Dirk Stroobandt. Epileptic seizure detection using reservoir computing. In *19th Annual Workshop on Circuits, Systems and Signal Processing*, 2008.

[9] Pieter Buteneers, David Verstraeten, Pieter van Mierlo, Tine Wyckhuys, Dirk Stroobandt, Robrecht Raedt, Hans Hallez, and Benjamin Schrauwen. Automatic detection of epileptic seizures on the intra-cranial electroencephalogram of rats using reservoir computing. *Artificial intelligence in medicine*, 53(3):215–223, 2011.

[10] Jose M Camara, Miquel Moreto, Enrique Vallejo, Ramon Beivide, Jose Miguel-Alonso, Carmen Martínez, and Javier Navaridas. Twisted torus topologies for enhanced interconnection networks. *Parallel and Distributed Systems, IEEE Transactions on*, 21(12):1765–1778, 2010.

[11] Aaron Carroll and Gernot Heiser. An analysis of power consumption in a smartphone. In *USENIX annual technical conference*, pages 1–14, 2010.

[12] Joseph Chrol-Cannon and Yaochu Jin. On the correlation between reservoir metrics and performance for time series classification under the influence of synaptic plasticity. *PLoS ONE*, 9(7):e101792, 07 2014.

[13] Leon Chua. Resistance switching memories are memristors. *Applied Physics A*, 102(4):765–783, 2011.

[14] L.O. Chua. Memristor-the missing circuit element. *Circuit Theory, IEEE Transactions on*, 18(5):507–519, Sep 1971.

[15] Roddy Cowie, Ellen Douglas-Cowie, Nicolas Tsapatsoulis, George Votsis, Stefanos Kollias, Winfried Fellenz, and John G Taylor. Emotion recognition in human-computer interaction. *Signal Processing Magazine, IEEE*, 18(1):32–80, 2001.

[16] Colin Donahue, Cory Merkel, Qutaiba Saleh, Levs Dolgovs, Yu Kee Ooi, Dhireesha Kudithipudi, and Bryant Wysocki. Design and analysis of neuromemristive echo state networks with limited-precision synapses. page Under print, 2015.

[17] Idongesit E. Ebong and Pinaki Mazumder. CMOS and memristor-based neural network design for position detection. *Proceedings of the IEEE*, 100(6):2050–2060, June 2012.

[18] Thomas E Gibbons. Unifying quality metrics for reservoir networks. In *Neural Networks (IJCNN), The 2010 International Joint Conference on*, pages 1–7. IEEE, 2010.

[19] Jennifer Hasler and Bo Marr. Finding a roadmap to achieve large neuromorphic hardware systems. *Frontiers in neuroscience*, 7, 2013.

[20] K Ishu, Tijn van Der Zant, Vlatko Becanovic, and P Ploger. Identification of motion with echo state network. In *OCEANS'04. MTTS/IEEE TECHNO-OCEAN'04*, volume 3, pages 1205–1210. IEEE, 2004.

[21] Herbert Jaeger. The echo state approach to analysing and training recurrent neural networks – with an erratum note. *Bonn, Germany: German National Research Center for Information Technology GMD Technical Report*, 148:34, 2001.

[22] Herbert Jaeger. Adaptive nonlinear system identification with echo state networks. In *Advances in neural information processing systems*, pages 593–600, 2002.

[23] Herbert Jaeger. *Tutorial on training recurrent neural networks, covering BPPT, RTRL, EKF and the" echo state network" approach*. GMD-Forschungszentrum Informationstechnik, 2002.

[24] Bekir Karlik, M Osman Tokhi, and Musa Alci. A fuzzy clustering neural network architecture for multifunction upper-limb prosthesis. *Biomedical Engineering, IEEE Transactions on*, 50(11):1255–1261, 2003.

[25] Kevin G Keenan, Dario Farina, Roberto Merletti, and Roger M Enoka. Influence of motor unit properties on the size of the simulated evoked surface emg potential. *Experimental brain research*, 169(1):37–49, 2006.

[26] KevinG. Keenan, Dario Farina, Roberto Merletti, and RogerM. Enoka. Influence of motor unit properties on the size of the simulated evoked surface emg potential. *Experimental Brain Research*, 169(1):37–49, 2006.

[27] Rami N Khushaba and Sarath Kodagoda. Electromyogram (emg) feature reduction using mutual components analysis for multifunction prosthetic fingers control. In *Control Automation Robotics & Vision (ICARCV), 2012 12th International Conference on*, pages 1534–1539. IEEE, 2012.

[28] Norito Kokubun, Masahiro Sonoo, Tomihiro Imai, Yumiko Arimura, Satoshi Kuwabara, Tetsuo Komori, Masahito Kobayashi, Takahide Nagashima, Yuki Hatanaka, Emiko Tsuda, et al. Reference values for voluntary and stimulated single-fibre emg using concentric needle electrodes: a multicentre prospective study. *Clinical Neurophysiology*, 123(3):613–620, 2012.

[29] Manjari S Kulkarni and Christof Teuscher. Memristor-based reservoir computing. In *Nanoscale Architectures (NANOARCH), 2012 IEEE/ACM International Symposium on*, pages 226–232. IEEE, 2012.

[30] Duygu Kuzum, Shimeng Yu, and HS Philip Wong. Synaptic electronics: materials, devices and applications. *Nanotechnology*, 24(38):382001, 2013.

[31] Kijoon Lee. Sample entropy, 2012. http://www.mathworks.com/matlabcentral/fileexchange/35784-sample-entropy.

[32] Robert Legenstein and Wolfgang Maass. Edge of chaos and prediction of computational performance for neural circuit models. *Neural Networks*, 20(3):323–334, 2007.

[33] Matilde Leonardi and T Bedirhan Ustun. The global burden of epilepsy. *Epilepsia*, 43(s6):21–25, 2002.

[34] Mantas LukošEvičIus and Herbert Jaeger. Reservoir computing approaches to recurrent neural network training. *Computer Science Review*, 3(3):127–149, 2009.

[35] Mantas Lukoševičius, Herbert Jaeger, and Benjamin Schrauwen. Reservoir computing trends. *KI-Künstliche Intelligenz*, 26(4):365–371, 2012.

[36] Wolfgang Maass, Thomas Natschlger, and Henry Markram. Real-time computing without stable states: A new framework for neural computation based on perturbations. *Neural Computation*, 14(11):2531 – 2560, 2002.

[37] Carlos Martinez, Ramón Beivide, Esteban Stafford, Miquel Moretó, and Ernst M Gabidulin. Modeling toroidal networks with the gaussian integers. *Computers, IEEE Transactions on*, 57(8):1046–1056, 2008.

[38] C. Mead. Neuromorphic electronic systems. *Proceedings of the IEEE*, 78(10):1629–1636, Oct 1990.

[39] Cory Merkel, Qutaiba Saleh, Colin Donahue, and Dhireesha Kudithipudi. Memristive reservoir computing architecture for epileptic seizure detection. *Procedia Computer Science*, 41(0):249 – 254, 2014. 5th Annual International Conference on Biologically Inspired Cognitive Architectures, 2014 {BICA}.

[40] David Norton and Dan Ventura. Improving liquid state machines through iterative refinement of the reservoir. *Neurocomputing*, 73(16):2893–2904, 2010.

[41] Yu V Pershin and Massimiliano Di Ventra. Spin memristive systems: Spin memory effects in semiconductor spintronics. *Physical Review B*, 78(11):113309, 2008.

[42] Angkoon Phinyomark, Franck Quaine, Sylvie Charbonnier, Christine Serviere, Franck Tarpin-Bernard, and Yann Laurillau. Emg feature evaluation for improving myoelectric pattern recognition robustness. *Expert Systems with Applications*, 40(12):4832–4840, 2013.

[43] Matthew D Pickett, Dmitri B Strukov, Julien L Borghetti, J Joshua Yang, Gregory S Snider, Duncan R Stewart, and R Stanley Williams. Switching dynamics in titanium dioxide memristive devices. *Journal of Applied Physics*, 106(7):074508, 2009.

[44] Jeyavijayan Rajendran, Harika Manem, Ramesh Karri, and Garrett S. Rose. An energy-efficient memristive threshold logic circuit. *IEEE Transactions on Computers*, 61(4):474–487, 2012.

[45] M.B.I. Reaz, M.S. Hussain, and F. Mohd-Yasin. Techniques of emg signal analysis: detection, processing, classification and applications. *Biological Procedures Online*, 8(1):11–35, 2006.

[46] MBI Reaz, MS Hussain, and Faisal Mohd-Yasin. Techniques of emg signal analysis: detection, processing, classification and applications. *Biological procedures online*, 8(1):11–35, 2006.

[47] Joshua S Richman and J Randall Moorman. Physiological time-series analysis using approximate entropy and sample entropy. *American Journal of Physiology-Heart and Circulatory Physiology*, 278(6):H2039–H2049, 2000.

[48] Ali Rodan and Peter Tino. Minimum complexity echo state network. *Neural Networks, IEEE Transactions on*, 22(1):131–144, 2011.

[49] Rodrigo Sacchi, Mustafa C Ozturk, Jose C Principe, Adriano AFM Carneiro, and Ivan Nunes da Silva. Water inflow forecasting using the echo state network: a brazilian case study. In *Neural Networks, 2007. IJCNN 2007. International Joint Conference on*, pages 2403–2408. IEEE, 2007.

[50] Qutaiba Saleh, Cory Merkel, Dhireesha Kudithipudi, and Bryant Wysocki. Memristive computational architecture of the echo state networks for real-time speech emotion recognition. page Under print, 2015.

[51] Klaus R Scherer, Tom Johnstone, and Gundrun Klasmeyer. Vocal expression of emotion. *Handbook of affective sciences*, pages 433–456, 2003.

[52] Stefan Scherer, Mohamed Oubbati, Friedhelm Schwenker, and Günther Palm. Real-time emotion recognition from speech using echo state networks. In *Artificial neural networks in pattern recognition*, pages 205–216. Springer, 2008.

[53] Carlo H Sequin. Doubly twisted torus networks for vlsi processor arrays. In *Proceedings of the 8th annual symposium on Computer Architecture*, pages 471–480. IEEE Computer Society Press, 1981.

[54] Mark D Skowronski and John G Harris. Automatic speech recognition using a predictive echo state network classifier. *Neural networks*, 20(3):414–423, 2007.

[55] Dmitri B Strukov, Gregory S Snider, Duncan R Stewart, and R Stanley Williams. The missing memristor found. *Nature*, 453(7191):80–3, May 2008.

[56] Abdulhamit Subasi, Mustafa Yilmaz, and Hasan Riza Ozcalik. Classification of emg signals using wavelet neural network. *Journal of neuroscience methods*, 156(1):360–367, 2006.

[57] Matthew H Tong, Adam D Bickett, Eric M Christiansen, and Garrison W Cottrell. Learning grammatical structure with echo state networks. *Neural Networks*, 20(3):424–432, 2007.

[58] Andres Upegui and Eduardo Sanchez. Evolving hardware with self-reconfigurable connectivity in xilinx fpgas. In *Adaptive Hardware and Systems, 2006. AHS 2006. First NASA/ESA Conference on*, pages 153–162. IEEE, 2006.

[59] Y. Li X. Jiang. A kind of audio data retrieval method based on mfcc[j]. *Computer and Digtal Engineering*, 36(9):19–21, 2008.

[60] Petros Xanthopoulos, Steffen Rebennack, Chang-Chia Liu, Jicong Zhang, Gregory Holmes, Basim Uthman, and Panos Pardalos. pages 14–19, 2010.

[61] Hong-Bo Xie, Tianruo Guo, Siwei Bai, and Socrates Dokos. Hybrid soft computing systems for electromyographic signals analysis: a review. *Biomedical engineering online*, 13:8, 2014.

[62] Yulu Yang, Akira Funahashi, Akiya Jouraku, Hiroaki Nishi, Hideharu Amano, and Toshinori Sueyoshi. Recursive diagonal torus: an interconnection network for massively parallel computers. *Parallel and Distributed Systems, IEEE Transactions on*, 12(7):701–715, 2001.

[63] Xu Zhang and Ping Zhou. Sample entropy analysis of surface emg for improved muscle activity onset detection against spurious background spikes. *Journal of Electromyography and Kinesiology*, 22(6):901–907, 2012.